
**International Geology Review**
Publication details, including instructions for authors and subscription information:
http://www.informaworld.com/smpp/title~content=t902953900

# Natural and experimental constraints on formation of the continental crust based on niobium-tantalum fractionation

Xing Ding [ab]; Craig Lundstrom [c]; Fang Huang [c]; Jie Li [c]; Zeming Zhang [d]; Xiaoming Sun [e]; Jinlong Liang [a];Weidong Sun [af]
[a] Key Laboratory of Isotope Geochronology and Geochemistry, Guangzhou Institute of Geochemistry, Chinese Academy of Sciences, Wushan, Guangzhou 510640, China [b] Graduate University of the Chinese Academy of Sciences, Beijing 100049, China [c] Department of Geology, University of Illinois at Urbana-Champaign, 245 NHB, 1301 W. Green St., IL 61801, USA [d] Institute of Geology, Chinese Academy of Geological Sciences, Beijing 10037, China [e] Department of Earth Sciences, Sun Yatsen University, Guangzhou 510275, China [f] Research Centre for Mineral Resources, School of Earth and Space Sciences, University of Science and Technology of China, Hefei, 230026, China

**To cite this Article** Ding, Xing , Lundstrom, Craig , Huang, Fang , Li, Jie , Zhang, Zeming , Sun, Xiaoming , Liang, Jinlong andSun, Weidong(2009) 'Natural and experimental constraints on formation of the continental crust based on niobium-tantalum fractionation', International Geology Review, 51: 6, 473 — 501
**To link to this Article: DOI:** 10.1080/00206810902759749
**URL:** http://dx.doi.org/10.1080/00206810902759749

*International Geology Review*
Vol. 51, No. 6, June 2009, 473–501

Taylor & Francis
Taylor & Francis Group

# Natural and experimental constraints on formation of the continental crust based on niobium–tantalum fractionation

Xing Ding[a,b], Craig Lundstrom[c], Fang Huang[c], Jie Li[c], Zeming Zhang[d], Xiaoming Sun[e], Jinlong Liang[a] and Weidong Sun[a,f]*

[a]*Key Laboratory of Isotope Geochronology and Geochemistry, Guangzhou Institute of Geochemistry, Chinese Academy of Sciences, Wushan, Guangzhou 510640, China;* [b]*Graduate University of the Chinese Academy of Sciences, Beijing 100049, China;* [c]*Department of Geology, University of Illinois at Urbana-Champaign, 245 NHB, 1301 W. Green St., IL 61801, USA;* [d]*Institute of Geology, Chinese Academy of Geological Sciences, No. 26 Baiwangzhuang Road, Beijing 10037, China;* [e]*Department of Earth Sciences, Sun Yatsen University, Guangzhou 510275, China;* [f]*Research Centre for Mineral Resources, School of Earth and Space Sciences, University of Science and Technology of China, Hefei, 230026, China*



(*Accepted 19 January 2009*)

Fractionation between Nb and Ta, elements generally regarded as geochemical 'identical twins', is a key to deciphering the formation of the continental crust (CC). Here we show that Nb/Ta of rutile grains in eclogitic rocks from the Chinese Continental Scientific Drilling (CCSD) project are remarkably heterogeneous but overall subchondritic at core depths of 100–700 m, and are less variable and mainly suprachondritic at core depths of 700–3025 m, indicating clear Nb/Ta fractionation across a subducted slab. To understand the potential mechanism of Nb/Ta fractionation within the subducted plate, we analysed by laser ablation ICPMS a thermal migration experiment in which a wet andesite was placed in a large thermal gradient (300°C/cm with ends ranging from 950–350°C) at 0.5Gpa. Results show that Nb, Ta and Ti, driven by the thermal gradient, preferentially migrate by diffusion through supercritical fluids into the cooler end of the experiment (at ∽650–350°C). Due to contrasting Nb and Ta thermal migration patterns, dramatic fractionation between Nb, Ta, and Ti took place in the cooler end. Experimental results are consistent with the measured Nb, Ta in rutile from CCSD drillhole samples. We consider that major fractionation between Nb, Ta must occur before rutile appears, most likely during the prograde blueschist to amphibole–eclogite transformation, when Ti is also mobile. Before rutile appears, partitioning between Ti-rich dominant minerals such as amphiboles and fluids in the hotter region where dehydration preferentially occurs, produces Nb–Ta–Ti-rich fluids with subchondritic Nb/Ta, and dehydration residues with suprachondritic Nb/Ta. Meanwhile, owing to evolution of the thermal gradient within the subducting slab, thermal migration of Nb, Ta, and Ti in aqueous fluids result in Nb, Ta, and Ti enrichment in the cooler region and depletion in the hotter region. As a result of high-pressure metamorphism, hydrous rutile-rich eclogites with overall subchondritic Nb/Ta form in the cooler region, whereas relatively anhydrous rutile-poor eclogites with

*Corresponding author. Email: weidongsun@gig.ac.cn

ISSN 0020-6814 print/ISSN 1938-2839 online

DOI: 10.1080/00206810902759749
http://www.informaworld.com

suprachondritic Nb/Ta form in the hotter region. Subsequently, partial melting of hydrous rutile-rich eclogites with initial subchondritic Nb/Ta at deeper levels transfers overall subchondritic Nb/Ta coupled with Nb, Ta, and Ti depletion characteristics to the CC, leaving dry rutile-poor eclogites with suprachondritic Nb/Ta and rutile-rich residual eclogites with overall, heterogeneous subchondritic Nb/Ta as a complementary reservoir to the CC.

**Keywords**: Nb/Ta fractionation; thermal gradient; contineutal crust; subduction; fluids; high pressure experiment; rutile



## Introduction

Formation of continental crust (CC) is one of the most important processes in planetary differentiation. It is, however, still widely debated regarding to how the CC formed its distinct geochemical compositions, in particular, its Nb and Ta characteristics, i.e. Nb–Ta depletion and subchondritic Nb/Ta. Models such as melting of subducted slabs in rutile-bearing eclogite or rutile-free amphibolite phases in the early history of the Earth (Foley *et al.* 2002; Martin 1999; Rapp *et al.* 2000, 2003; Rapp and Watson 1995; Rudnick *et al.* 2000; Xiong 2006), arc magmatism and following intracrustal differentiation (Davidson and Turner 2006; Draut *et al.* 2002; Foden and Green 1992; Tatsumi *et al.* 2006), dehydration of subducting slabs and subsequently mass transportation by fluids (Collerson and Fryer 1978; Ionov and Hofmann 1995; Keppler 1996) and dehydration melting of subducted slabs (Kamber *et al.* 2002; Xiao *et al.* 2006), have been proposed.

Niobium and Ta have long been regarded as geochemical 'identical twins' because of their similar geochemical behaviours during processes linked to the evolution of the Earth's mantle (Green 1995; Jochum *et al.* 1986, 1989; Rudnick *et al.* 2000; Sun and McDonough 1989) due to identical valence states (+5) and similar atomic radii for octahedral coordination (Shannon 1976). However, the average Nb/Ta value of the CC is estimated to be about 12–13 (Barth *et al.* 2000; Plank and Langmuir 1998; Rudnick *et al.* 2003), much lower than that of the primitive mantle, i.e. 17.5 (McDonough and Sun 1995) or 19.9 (Munker *et al.* 2003), indicating major fractionation between Nb and Ta during the formation of the CC.

Given that at least 80% of the CC was likely generated at convergent margins (Barth *et al.* 2000; Rudnick *et al.* 2003), whereas subduction of oceanic lithosphere is one of the most important mass transportation processes in the silicate Earth, slab melting has long been considered the dominant scheme for the formation of the CC (Barth *et al.* 2002; Foley *et al.* 2002; McDonough 1991; Rudnick *et al.* 2000; Xiao *et al.* 2006; Xiong 2006). Slab melting in the presence of rutile can feasibly interpret the Ti, Nb, and Ta deficiency of the CC (McDonough 1991) since rutile is the main primary carrier of Nb and Ta (Green 1995; Zack *et al.* 2002) and a very common minor phase in the high-grade metamorphic system (Carswell *et al.* 1996; Liou *et al.* 1998b; Spandler *et al.* 2003; Tsujimori 2002; Zack *et al.* 2002). This model is supported by the observations of superchondritic Nb/Ta in kimberlitic eclogite xenoliths, which are thought to be residue of partially melted subducted oceanic slabs stored in the mantle (Rudnick *et al.* 2000). Experiments, however, show that rutile preferentially incorporates Ta over Nb (Foley *et al.* 2000; Klemme *et al.* 2005; Schmidt *et al.* 2004; Xiong *et al.* 2005), such that melts from a rutile-bearing oceanic slab should have even higher Nb/Ta than that of MORB and the residue, which cannot reconcile subchondritic Nb/Ta of the CC (Foley *et al.* 2002). Although melting of hydrous rutile-bearing eclogites with initially low Nb/Ta

ratios can produce subchondritic Nb/Ta characteristics (Rapp *et al.* 2003; Xiong 2006; Xiong *et al.* 2005), sources such as arc crust and very depleted mid-oceanic ridge basalts (Niu and Batiza 1997; Rapp *et al.* 2003; Sun *et al.* 2003) are not volumetrically important enough to quantitatively account for the low Nb/Ta of the CC. Therefore, a simple model of melting of the subducted slab cannot convincingly explain the Nb and Ta characteristics of the CC.

Based on highly fractionated Nb/Ta in rutile grains collected from a CCSD pilot drill hole at the depth of 180 m, a 'zone refining' dehydration model was proposed, suggesting that major Nb/Ta fractionation occurs in the absence of rutile during blueschist to amphibolite transformation, resulting in low Nb/Ta in hydrous eclogites in cool regions which supply crucial sources on forming subchondritic Nb/Ta of the CC (Xiao *et al.* 2006). Major Nb/Ta fractionation within ultrahigh pressure metamorphic rocks has been confirmed by later studies (Liang *et al.* 2008; Zhang *et al.* 2008). Nevertheless, this model was built on limited samples and data, e.g. the suprachondritic hot region in the slab was not well illustrated (Xiao *et al.* 2006). In this paper, we systematically studied the Nb and Ta concentrations of rutile grains from CCSD eclogites in depths ranging from 100 to 3025 m, and documented obvious Nb/Ta fractionation in the profile of a subducted crust that exhumated from depths of more than 100 km in the Triassic (Li *et al.* 1993; Ye *et al.* 2000). Meanwhile, to understand the potential mechanism of Nb and Ta fractionation, we analysed a thermal migration experiment from Huang *et al.* (2009) to understand the fractionation of Nb and Ta under a temperature gradient.



## Nb/Ta fractionation in natural rutile from the CCSD

### *Geological setting and samples*

The CCSD is located in Donghai County, Jiangsu Povince, Eastern China (Xu 2004). It was designed to drill through the Sulu–Dabie ultrahigh-pressure (UHP) metamorphic belt (Xu 2004; Xu *et al.* 1998), which is the largest UHP terrain so far found worldwide (Figure 1A). The Sulu–Dabie UHP belt was formed during the collision between the North China Block and the South China Block (Li *et al.* 1993, 2000; Sun *et al.* 2002; Zhang *et al.* 1995; Zheng *et al.* 2003). It reached its peak metamorphism at ca. 226 $\pm$ 2 Myrs ago (Li *et al.* 1993, 1994; Liu *et al.* 2006a). Studies show that the continental crust subducted to depths of greater than 100 km (Ye *et al.* 2000; Zhang and Liou 1996), and then uplifted rapidly back to the upper CC (You *et al.* 2005; Zhang *et al.* 2005b,c) as a whole (Wang *et al.* 2008; Zhang *et al.* 2005c), which provides ideal samples to directly observe chemical changes within the subducted crust (Liu *et al.* 2006b; Su *et al.* 2005).

Mineralogy and petrology of the Sulu–Dabie UHP belt had been a hot topic for more than 20 years (Kato *et al.* 1997; Su *et al.* 2005; Sun *et al.* 2007; Tong *et al.* 2007; Wang *et al.* 1989; Ye *et al.* 2000; You *et al.* 2004, 2005; Zhang *et al.* 1995, 2005a, 2000, 2008). In brief, the main drillhole of the CCSD (0–3050 m) consists mainly of eclogites with a total thickness of greater than 1300 m, alternated with associated rocks such as garnet peridotite, paragneiss, orthogneiss, schist and quartzite (Figure 1B). Due to obvious variations of major and trace element abundances, the main hole eclogites of the CCSD were classified into high-Si, high-Al, high-Mg, high-Ti, high-Ti-Fe and normal types (Zhang *et al.* 2004). High-Ti eclogites, mainly situated at depths of about 300–600 m, have abundant rutile whereas high-Ti–Fe

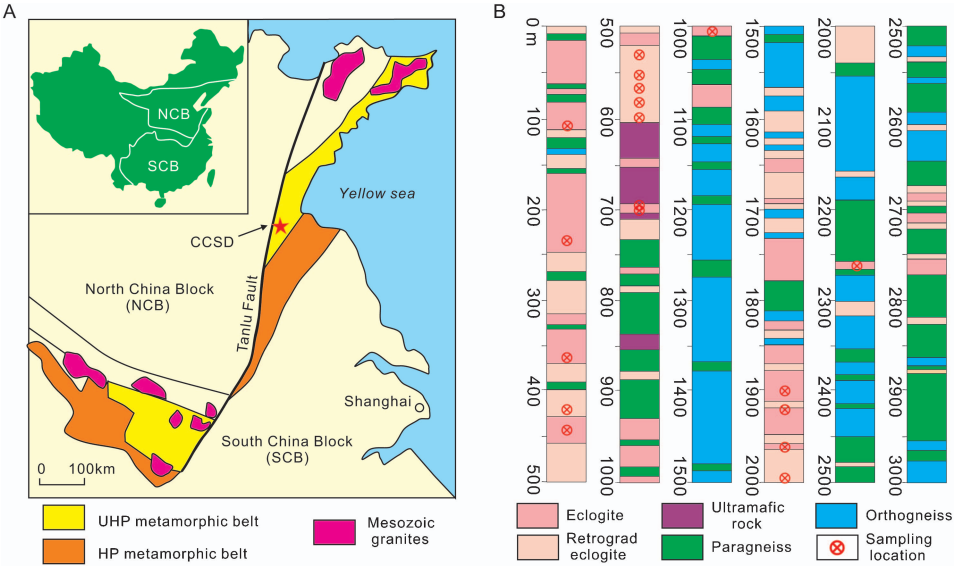


Figure 1. (A) Map of the CCSD site located in the largest ultrahigh-pressure metamorphic belt, the Dabie–Sulu orogenic belt, which is the result of a collision that occurred ca. 226 Myrs ago between the NCB and the SCB. (B) Simplified lithological profile of the main hole core of the CCSD showing the sampling locations.

eclogites have few rutile but abundant ilmenite and Ti-bearing magnetite (Wang *et al.* 2005; Zhang *et al.* 2004).

In this work, 19 thin sections of investigated rutile-bearing eclogite samples were collected from the main CCSD drillhole core (100–3025 m). The eclogite samples consist mainly of garnet, omphacite, and accessory minerals including rutile, phengite, amphibole, quartz or coesite, kyanite, ± epidote, chlorite, plagioclase, apatite, zircon, titanite, and ilmenite. Rutile in all samples occurs as euhedral to subhedral grains (Figure 2A), with diameters ranging from about 10 μm up to more than 1000 μm. Correspondingly, the rutile grains in high-Ti eclogites are much bigger and more euhedral. Most rutile grains are included in major metamorphic minerals like garnet, omphacite, or phengite (Figure 2A and B) with some intergranular grains (Figure 2A). As a track record of high pressure metamorphism, a few rutile grains have inclusions, including garnet, omphacite, and some minor minerals such as pargasite, zircon, and clinozoisite. Also, a few rutile grains in retrograde eclogites are surrounded by ilmenite and/or titanite, representing the retrograde metamorphic results.

### *Analytical method*

Eclogite samples were cut and polished as thin sections with a thickness of up to 0.5 mm. Sixty-eight rutile grains with different granularities and shapes but no or a minor retrograde rim were then selected based on careful study under the microscope for mineral analysis and composition measurement. After trace element measurement, selected rutile grains in the thin sections were checked again by scanning electronic microscope (SEM), in order to ensure that the measurements were done indeed on rutile, rather than retrograde rim or other minerals (Figure 2B–D).

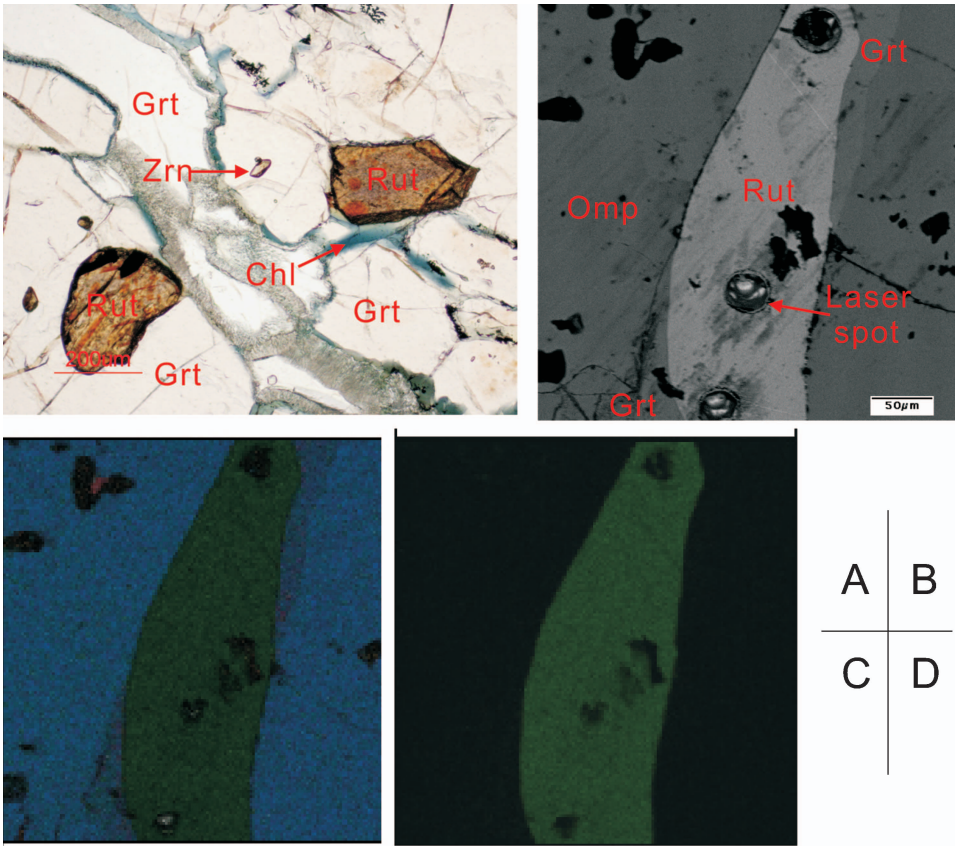


Figure 2. (A) A photomicrograph of an investigated eclogite (sample no. B162R140P1f) showing euhedral rutile and surrounding minerals. (B) BSE image of an investigated rutile grain for LA-ICP-MS analysis spots (rutile no. 24). (C) X-ray phase map showing that rutile grains are surrounded by garnet and omphacite and have few inclusions. (D) Ti X-ray map showing that rutile grains have no retrograde rim. Chl, chlorite; Grt, garnet; Omp, omphacite; Rut, rutile; Zrn, zircon.

Mineral/inclusion identification and major element determination for thin sections were done by electron microprobe analysis (EMPA) on a JEOL JXA-8100 Superprobe, using an accelerating voltage of 15.0 kV, beam current of 10 nA, and spot diameter of 1 μm, at Guangzhou Institute of Geochemistry, the Chinese Academy of Sciences. Both silicates and pure oxides were used as standards. Rutile major element compositions and phase scan were completed by the average of two standards-based energy dispersive (EDS) X-ray analyses using a 250 $\mu m^2$ raster on the JEOL 840A SEM in the Department of Geology, University of Illinois at Urbana-Champaign. The acceleration voltage during analysis was 15 kV and beam current was 30 nA.

Nb and Ta concentrations were determined using laser ablation inductively coupled plasma mass spectrometer (LA-ICP-MS) at the State Key Laboratory of Continental Dynamics, Northwest University. The system consists of an Agilent 7500 ICP-MS coupled with a GeoLas200M ArF-Excimer laser source ($\lambda$=193 nm) with repetition rate of 20 Hz and beam energy of 200 mJ. Diameter of laser spot was 30 μm, and the ablated aerosol was carried to the ICP source with He gas. $^{49}$Ti was

used as an internal standard, and NIST610 was used as an external calibration standard. Reproducibility of trace element concentrations is better than 10%.

### *Analytical results*

Using a LA-ICP-MS, we analysed the Nb and Ta concentrations of 68 rutile grains from CCSD eclogites in depths ranging from 100 to 3025 m. All together, 143 analyses were carried out (Table 1). Generally, the data show following characteristics.

*Large Nb, Ta and Nb/Ta variations along the drill hole*

As shown in Figure 3A and B, the Nb, Ta concentrations and Nb/Ta vary significantly along the drillhole. The Nb and Ta concentrations range from 6.30 to 1636 and 0.36 to 81.1 ppm (Table 1), with average values of 214 and 9.62 ppm, respectively. The Nb and Ta average values are lower than those in rutile from eclogites and garnet mica schists of the central Alps (Nb=470 ppm; Ta=21.1 ppm) (Zack *et al.* 2002), but a little higher than those in rutile from coesite-bearing eclogites from Roberts Victor kimberlite (Nb=108 ppm; Ta=7.66 ppm), which is interpreted as a recycled late Archean oceanic crust (Jacob *et al.* 2003). Correspondingly, Nb/Ta also shows significant fractionation, varying from 7.45 to 46.4 (Table 1), with an average value of 21.5. In general, rutile grains have high Nb and Ta concentrations and overall suprachondritic Nb/Ta at depths above 180 m. At depths between 180 and 700 m, the concentrations are remarkably lower, with more than 70% of the analysed samples having subchondritic values. By contrast, at depths greater than 700 m, both Nb and Ta concentrations and Nb/Ta in rutile are less varied, and about 80% of the analysed samples have suprachondritic Nb/Ta.

*Dramatic differences between rutiles in eclogites and associated quartz veins*

The Nb and Ta concentrations in rutile from a quartz vein sample at a depth of 180 m, vary from 660 to 2080 and 28.6 to 235 ppm, with average values of 1564 and 159 ppm, respectively (Xiao *et al.* 2006). As seen in Figure 3A, most Nb and Ta concentrations for rutile from the quartz vein at a depth of 180 m are over two times higher than those from eclogites. Interestingly, Nb/Ta from the quartz vein sample range from 6.2 to 29.1, with an average value of 10.4, showing overall subchondritic Nb/Ta, which is much lower than that from eclogites in this study (Figure 3B).

*Similar Nb, Ta and Nb/Ta distributions within the same rutile grain and between grains at the same depth*

As seen in Figure 4, no big differences in Nb or Ta concentration in a single grain for most rutile occur among the rim, mantle, and core, except for individual samples at depths of 108, 690, and 1993 m. Due to homogeneous Nb and Ta distributions in a single grain, Nb/Ta among the rim, mantle, and core in most rutile shows limited fractionation (Table 1). Nb and Ta concentrations and Nb/Ta ratios also have no obvious differences between grains at the same depth (Figure 4 and Table 1).

In contrast to most other grains, rutile grains at depths of 108, 690, and 1993 m show Nb and Ta zonation, e.g. Nb and Ta concentrations increase from the core to the rim. Moreover, the overall Nb and Ta concentrations are much higher than those in nearby samples. Similar phenomena were reported in the quartz vein samples at depths of about 180 m (Xiao *et al.* 2006), interpreted as limited retrograde metamorphic effects.

Table 1. Nb and Ta concentrations of rutile grains from CCSD eclogites (in ppm).

| Sample no. | Spot no. | Rutile no. | Location* | depth | Nb | 1σ | Ta | 1σ | Nb/Ta |
|---|---|---|---|---|---|---|---|---|---|
| B4R8P1 | 1J1 | 1 | R | 108.7 | 635 | 19.5 | 24.8 | 0.78 | 25.6 |
| | 1J2 | | R | 108.7 | 633 | 19.4 | 25.6 | 0.81 | 24.7 |
| | 1J3 | | R | 108.7 | 660 | 20.3 | 26.3 | 0.83 | 25.1 |
| | 1J4 | | R | 108.7 | 1636 | 50.3 | 58.0 | 1.84 | 28.2 |
| | 2J1 | 2 | C | 108.7 | 726 | 22.4 | 30.5 | 0.97 | 23.8 |
| | 2J2 | | R | 108.7 | 672 | 20.8 | 30.0 | 0.97 | 22.4 |
| | 2J3 | 3 | R | 108.7 | 677 | 21.0 | 29.6 | 0.97 | 22.9 |
| | 2J4 | | R | 108.7 | 682 | 21.2 | 28.7 | 0.95 | 23.8 |
| | 2J5 | | R | 108.7 | 708 | 22.0 | 27.7 | 0.92 | 25.6 |
| B132R114P1CL | 1J7 | 4 | C | 235.2 | 59.4 | 1.83 | 2.39 | 0.08 | 24.8 |
| | 1J8 | | R | 235.2 | 57.2 | 1.78 | 2.62 | 0.10 | 21.8 |
| | 1J9 | 5 | C | 235.2 | 57.0 | 1.76 | 2.37 | 0.08 | 24.1 |
| | 1J10 | | R | 235.2 | 60.9 | 1.88 | 2.45 | 0.09 | 24.8 |
| | 3J1 | | R | 235.2 | 55.3 | 1.76 | 1.68 | 0.08 | 32.9 |
| | 3J2 | 6 | C | 235.2 | 55.2 | 1.77 | 1.65 | 0.08 | 33.4 |
| | 3J3 | | R | 235.2 | 57.3 | 1.83 | 1.66 | 0.08 | 34.5 |
| B162R140P1f | 1J1 | | R | 369.0 | 154 | 4.98 | 7.89 | 0.25 | 19.5 |
| | 1J2 | 7 | R–M | 369.0 | 155 | 5.04 | 5.83 | 0.19 | 26.6 |
| | 1J3 | | R | 369.0 | 158 | 5.14 | 7.34 | 0.24 | 21.5 |
| | 1J4 | | R | 369.0 | 150 | 4.95 | 10.5 | 0.36 | 14.3 |
| | 1J5 | | R | 369.0 | 172 | 5.65 | 7.88 | 0.25 | 21.8 |
| | 1J6 | 8 | C | 369.0 | 155 | 5.12 | 6.75 | 0.22 | 23.0 |
| | 1J7 | | M | 369.0 | 157 | 5.24 | 7.34 | 0.24 | 21.4 |
| | 1J8 | | R | 369.0 | 162 | 5.43 | 8.71 | 0.28 | 18.6 |
| | 2J1 | | R | 369.0 | 159 | 5.46 | 7.91 | 0.26 | 20.2 |
| | 2J2 | | R | 369.0 | 159 | 5.48 | 7.56 | 0.25 | 21.0 |
| | 2J3 | 9 | M–C | 369.0 | 159 | 5.55 | 6.91 | 0.23 | 23.0 |
| | 2J4 | | C–M | 369.0 | 161 | 5.70 | 7.44 | 0.24 | 21.6 |
| | 2J5 | | R | 369.0 | 184 | 6.58 | 7.59 | 0.25 | 24.2 |

Table 1. (*Continued.*)

| Sample no. | Spot no. | Rutile no. | Location* | depth | Nb | 1σ | Ta | 1σ | Nb/Ta |
|---|---|---|---|---|---|---|---|---|---|
| B199R176P6i | 1J1 | | R | 433.0 | 134 | 5.18 | 8.28 | 0.33 | 16.2 |
| | 1J2 | | R | 433.0 | 157 | 6.10 | 8.05 | 0.32 | 19.5 |
| | 1J3 | 10 | M | 433.0 | 137 | 5.38 | 8.30 | 0.34 | 16.5 |
| | 1J4 | | C | 433.0 | 138 | 5.52 | 8.41 | 0.35 | 16.4 |
| | 1J5 | | R | 433.0 | 134 | 5.47 | 8.98 | 0.38 | 14.9 |
| | 2J1 | 11 | C | 433.0 | 142 | 5.92 | 8.99 | 0.38 | 15.8 |
| | 2J2 | 12 | R | 433.0 | 148 | 6.34 | 9.59 | 0.42 | 15.4 |
| | 2J3 | 13 | C–R | 433.0 | 146 | 6.43 | 9.35 | 0.42 | 15.6 |
| | 3J1 | 14 | R | 433.0 | 147 | 6.89 | 9.25 | 0.45 | 15.9 |
| | 3J2 | | C | 433.0 | 141 | 6.86 | 8.81 | 0.44 | 16.0 |
| B208R185P1e | 1J1 | 15 | R | 448.0 | 38.1 | 2.41 | 2.22 | 0.09 | 17.2 |
| | 1J2 | | M | 448.0 | 38.3 | 2.49 | 2.40 | 0.09 | 16.0 |
| | 1J3 | | C | 448.0 | 40.4 | 1.89 | 2.74 | 0.10 | 14.8 |
| | 1J4 | | M | 448.0 | 39.0 | 1.83 | 2.58 | 0.10 | 15.2 |
| | 1J5 | | R | 448.0 | 38.9 | 1.82 | 2.41 | 0.09 | 16.1 |
| | 1J6 | | R | 448.0 | 41.6 | 1.96 | 1.80 | 0.07 | 23.1 |
| | 1J7 | | R | 448.0 | 40.0 | 1.91 | 2.00 | 0.08 | 20.1 |
| | 1J8 | 16 | C | 448.0 | 37.8 | 1.82 | 2.52 | 0.09 | 15.0 |
| | 1J9 | | M | 448.0 | 38.2 | 1.87 | 2.54 | 0.10 | 15.0 |
| | 1J10 | | R | 448.0 | 35.9 | 1.79 | 1.86 | 0.08 | 19.3 |
| | 2J1 | 17 | R | 448.0 | 41.1 | 2.14 | 2.36 | 0.09 | 17.4 |
| | 3J1 | | R | 448.0 | 50.1 | 2.65 | 2.47 | 0.09 | 20.3 |
| | 3J2 | | M | 448.0 | 44.0 | 2.38 | 2.33 | 0.09 | 18.9 |
| | 3J3 | 18 | C | 448.0 | 44.1 | 2.45 | 2.49 | 0.09 | 17.7 |
| | 3J4 | | M | 448.0 | 45.5 | 2.59 | 2.56 | 0.10 | 17.8 |
| | 3J5 | | R | 448.0 | 44.8 | 2.62 | 2.60 | 0.10 | 17.2 |

Table 1. (*Continued.*)

| Sample no. | Spot no. | Rutile no. | Location* | depth | Nb | 1σ | Ta | 1σ | Nb/Ta |
|---|---|---|---|---|---|---|---|---|---|
| B261R222P1a | 2J1 | | R | 531.5 | 85.1 | 2.63 | 3.26 | 0.11 | 26.1 |
| | 2J2 | 19 | M | 531.5 | 83.8 | 2.59 | 3.27 | 0.12 | 25.6 |
| | 2J3 | | C | 531.5 | 82.3 | 2.55 | 3.17 | 0.12 | 26.0 |
| | 2J4 | | M–R | 531.5 | 85.3 | 2.64 | 3.21 | 0.12 | 26.6 |
| | 2J5 | | R | 531.5 | 86.2 | 2.68 | 3.63 | 0.13 | 23.7 |
| | 2J6 | | R | 531.5 | 81.2 | 2.51 | 3.12 | 0.11 | 26.0 |
| | 2J7 | 20 | C | 531.5 | 84.8 | 2.63 | 3.43 | 0.13 | 24.7 |
| | 2J8 | | M | 531.5 | 83.2 | 2.58 | 3.49 | 0.13 | 23.8 |
| | 2J9 | 21 | R–C | 531.5 | 83.6 | 2.60 | 3.47 | 0.13 | 24.1 |
| | 3J1 | 22 | R | 531.5 | 91.3 | 2.83 | 3.37 | 0.12 | 27.1 |
| B278R230P3f | 1J1 | | R | 558.7 | 15.1 | 0.50 | 0.90 | 0.04 | 16.9 |
| | 1J2 | 23 | C–R | 558.7 | 14.5 | 0.48 | 0.83 | 0.04 | 17.5 |
| | 1J3 | | C–R | 558.7 | 14.4 | 0.48 | 0.96 | 0.04 | 15.1 |
| | 1J4 | | R | 558.7 | 26.3 | 0.85 | 1.08 | 0.05 | 24.2 |
| | 2J1 | | R | 558.7 | 13.2 | 0.44 | 0.56 | 0.03 | 23.5 |
| | 2J2 | 24 | C | 558.7 | 14.6 | 0.49 | 0.63 | 0.04 | 23.1 |
| | 2J3 | | R | 558.7 | 14.7 | 0.49 | 0.70 | 0.04 | 20.9 |
| B282R232P1h | 1J1 | | R | 565.2 | 17.4 | 0.69 | 0.98 | 0.06 | 17.7 |
| | 1J2 | 25 | C | 565.2 | 21.5 | 0.80 | 1.33 | 0.07 | 16.2 |
| | 1J3 | | C | 565.2 | 21.4 | 0.83 | 1.16 | 0.07 | 18.4 |
| | 1J4 | | R | 565.2 | 25.3 | 0.99 | 1.66 | 0.09 | 15.3 |
| | 1J5 | 26 | M | 565.2 | 37.2 | 1.40 | 3.82 | 0.17 | 9.7 |
| | 1J6 | | R | 565.2 | 41.3 | 1.56 | 5.54 | 0.22 | 7.45 |
| | 2J1 | 27 | M | 565.2 | 162 | 6.04 | 8.45 | 0.30 | 19.2 |
| | 2J2 | | R | 565.2 | 126 | 4.81 | 7.83 | 0.29 | 16.1 |
| | 2J3 | 28 | M | 565.2 | 126 | 4.93 | 8.02 | 0.30 | 15.7 |

Table 1. (*Continued.*)

| Sample no. | Spot no. | Rutile no. | Location* | depth | Nb | 1σ | Ta | 1σ | Nb/Ta |
|---|---|---|---|---|---|---|---|---|---|
| B287R235P1b | 1J1 | | R | 572.2 | 11.8 | 0.40 | 0.63 | 0.04 | 18.7 |
| | 1J2 | 29 | M | 572.2 | 10.2 | 0.34 | 0.57 | 0.03 | 17.9 |
| | 1J3 | | C–R | 572.2 | 10.6 | 0.36 | 0.57 | 0.03 | 18.4 |
| | 1J4 | | R | 572.2 | 10.4 | 0.40 | 0.62 | 0.04 | 16.7 |
| | 2J1 | 30 | C–M | 572.2 | 11.4 | 0.38 | 0.49 | 0.03 | 23.3 |
| | 2J2 | | R | 572.2 | 11.1 | 0.37 | 0.50 | 0.03 | 22.0 |
| | 2J3 | 31 | R | 572.2 | 11.4 | 0.38 | 0.54 | 0.03 | 21.0 |
| B301R246P4b | 1J1 | 32 | R | 596.6 | 6.54 | 0.23 | 0.45 | 0.03 | 14.7 |
| | 1J2 | 33 | C | 596.6 | 6.91 | 0.26 | 0.37 | 0.03 | 18.7 |
| | 1J3 | 34 | R | 596.6 | 6.41 | 0.23 | 0.36 | 0.02 | 17.7 |
| | 2J1 | | R | 596.6 | 6.76 | 0.26 | 0.44 | 0.03 | 15.3 |
| | 2J2 | 35 | C | 596.6 | 6.68 | 0.24 | 0.44 | 0.03 | 15.3 |
| | 2J3 | | R | 596.6 | 6.30 | 0.23 | 0.37 | 0.02 | 16.8 |
| B353R283P1j | 2J1 | 36 | R | 687.7 | 42.89 | 1.35 | 1.35 | 0.06 | 31.68 |
| B356R284P1h | 1J1 | 37 | R–M | 690.1 | 93.5 | 2.89 | 3.80 | 0.13 | 24.6 |
| | 1J2 | 38 | R–C | 690.1 | 96.2 | 2.98 | 3.23 | 0.12 | 29.8 |
| | 2J1 | 39 | R | 690.1 | 114 | 3.51 | 4.63 | 0.16 | 24.6 |
| B552R399P1L | 1J2 | | M | 1003.4 | 465 | 49.7 | 18.0 | 1.86 | 25.9 |
| | 1J3 | | C–M | 1003.4 | 520 | 63.2 | 19.3 | 2.26 | 26.9 |
| | 1J4 | 40 | M | 1003.4 | 518 | 72.2 | 19.3 | 2.58 | 26.9 |
| | 1J5 | | R | 1003.4 | 494 | 78.6 | 18.7 | 2.86 | 26.4 |
| | 1J6 | 41 | R | 1003.4 | 534 | 96.5 | 19.4 | 3.35 | 27.6 |
| | 1J7 | | C | 1003.4 | 483 | 98.0 | 17.5 | 3.39 | 27.7 |
| | 2J1 | 42 | R | 1003.4 | 666 | 150 | 14.3 | 3.10 | 46.4 |
| | 2J2 | | M | 1003.4 | 439 | 109 | 13.7 | 3.27 | 32.0 |
| | 2J3 | 43 | C | 1003.4 | 447 | 132 | 12.8 | 3.63 | 34.8 |
| | 2J4 | | R | 1003.4 | 486 | 156 | 22.2 | 6.78 | 21.9 |
| | 2J5 | | C | 1003.4 | 452 | 156 | 16.8 | 5.53 | 26.8 |
| | 2J6 | 44 | C | 1003.4 | 448 | 165 | 18.8 | 6.61 | 23.8 |
| | 2J7 | | R | 1003.4 | 646 | 254 | 19.2 | 7.17 | 33.8 |

Table 1. (*Continued.*)

| Sample no. | Spot no. | Rutile no. | Location* | depth | Nb | 1σ | Ta | 1σ | Nb/Ta |
|---|---|---|---|---|---|---|---|---|---|
| B993R636P8p | 1J1 | 45 | R | 1901.1 | 346 | 10.7 | 15.4 | 0.53 | 22.5 |
| | 1J2 | 46 | R | 1901.1 | 372 | 11.5 | 17.3 | 0.59 | 21.5 |
| | 1J3 | 47 | M–C | 1901.1 | 399 | 12.3 | 17.0 | 0.58 | 23.4 |
| | 1J4 | 48 | R | 1901.1 | 478 | 14.7 | 18.1 | 0.61 | 26.4 |
| | 2J1 | | R | 1901.1 | 404 | 12.5 | 17.8 | 0.60 | 22.7 |
| | 2J2 | 49 | R | 1901.1 | 460 | 14.0 | 21.8 | 0.67 | 21.1 |
| | 2J3 | | C–M | 1901.1 | 385 | 11.8 | 18.1 | 0.56 | 21.3 |
| | 2J4 | 50 | R–M | 1901.1 | 408 | 12.4 | 17.2 | 0.53 | 23.7 |
| | 2J5 | 51 | C–M | 1901.1 | 393 | 12.0 | 19.6 | 0.60 | 20.0 |
| B1011R640P2o | 3J1 | 52 | R–C | 1928.6 | 236 | 7.22 | 11.0 | 0.35 | 21.4 |
| | 3J2 | 53 | R | 1928.6 | 239 | 7.30 | 10.8 | 0.34 | 22.1 |
| B1033R645P6Q | 2J1 | 54 | | 1964.4 | 203 | 6.22 | 9.26 | 0.30 | 21.9 |
| | 2J2 | | | 1964.4 | 209 | 6.39 | 9.79 | 0.31 | 21.3 |
| B1049R648P28d | 1J2 | 55 | M | 1992.7 | 1017 | 36.9 | 81.1 | 2.60 | 12.6 |
| | 1J3 | 56 | R | 1992.7 | 464 | 14.8 | 28.7 | 0.94 | 16.2 |
| | 1J4 | | C | 1992.7 | 316 | 9.76 | 24.1 | 0.75 | 13.1 |
| | 2J5 | 57 | R | 1992.7 | 221 | 6.76 | 9.46 | 0.30 | 23.4 |
| | 2J6 | | M | 1992.7 | 224 | 6.85 | 10.7 | 0.33 | 21.1 |
| | 2J7 | | R–M | 1992.7 | 232 | 7.09 | 10.2 | 0.32 | 22.7 |
| | 2J8 | 58 | C | 1992.7 | 229 | 6.98 | 9.50 | 0.30 | 24.1 |
| | 2J9 | | R | 1992.7 | 223 | 6.83 | 10.2 | 0.33 | 21.9 |
| B1156R61P24 | 1J1 | 59 | R | 2269.2 | 229 | 6.99 | 9.10 | 0.29 | 25.2 |
| | 1J2 | 60 | R | 2269.2 | 217 | 6.70 | 9.22 | 0.31 | 23.6 |
| | 1J3 | 61 | C | 2269.2 | 218 | 6.66 | 9.50 | 0.30 | 23.0 |
| | 3J1 | 62 | C–R | 2269.2 | 195 | 5.97 | 9.75 | 0.31 | 20.0 |
| | 3J2 | 63 | R | 2269.2 | 225 | 6.87 | 9.72 | 0.31 | 23.1 |
| | 3J3 | 64 | C | 2269.2 | 210 | 6.42 | 10.3 | 0.32 | 20.4 |
| | 3J4 | 65 | R | 2269.2 | 221 | 6.74 | 10.2 | 0.32 | 21.8 |
| B1539R7P12 | 2J1 | 66 | R–C | 3025.6 | 411 | 12.5 | 18.7 | 0.58 | 22.0 |
| | 2J2 | 67 | C | 3025.6 | 438 | 13.4 | 19.5 | 0.61 | 22.5 |
| | 3J1 | 68 | C–R | 3025.6 | 388 | 11.8 | 24.1 | 0.74 | 16.1 |

Note: *Location of laser spot on the rutile: R=rim, M=mantle, C=core.

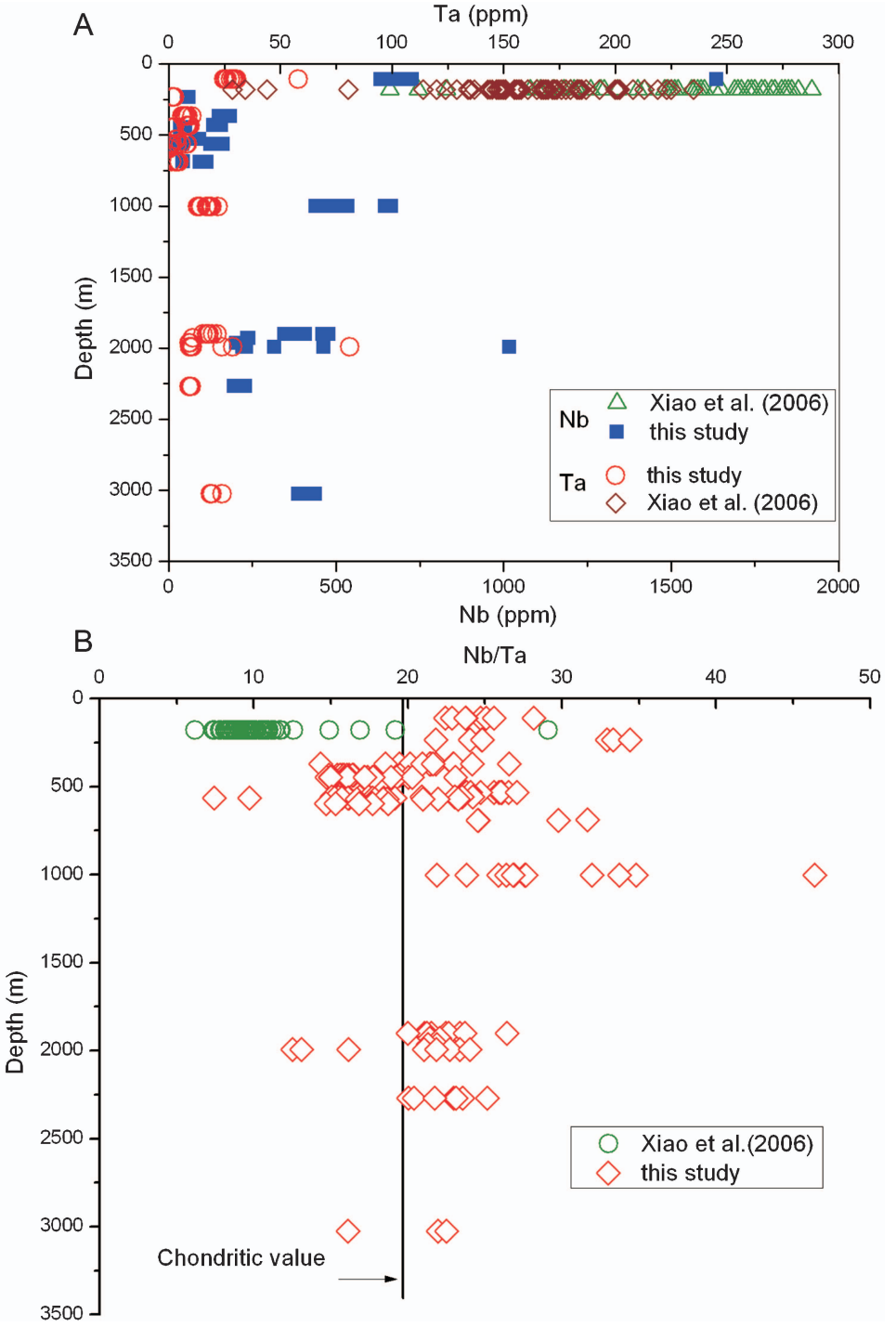


Figure 3. (A) Depth of investigated rutile grains versus Nb and Ta. (B) Depth of investigated rutile grains versus Nb/Ta. Data source: Table 1, and the data on quartz vein from the pilot drill hole of the CCSD (Xiao *et al.* 2006).

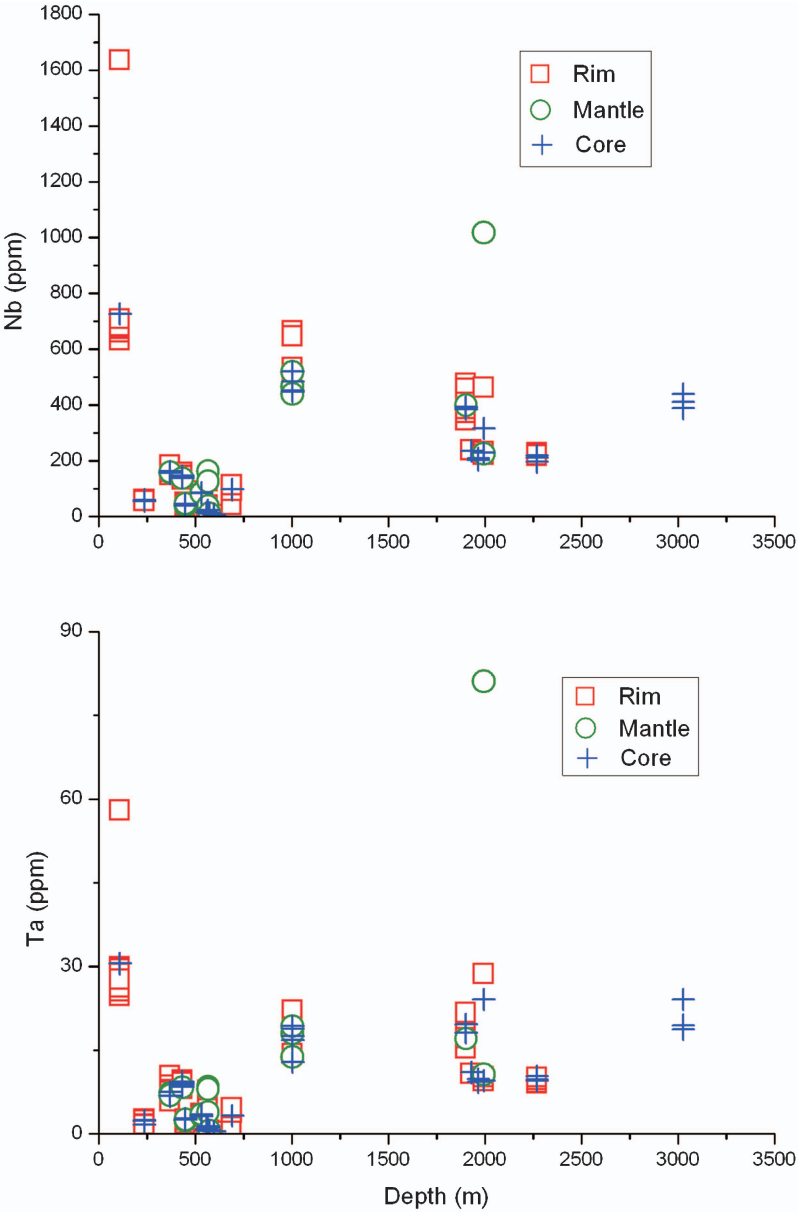


Figure 4. Nb and Ta concentration distributions among the rim, mantle, and core in the investigated rutile grains.

## Nb/Ta fractionation during a thermal migration experiment

Considering its thickness and heterogeneity in temperature and water contents during subduction (Abers *et al.* 2006; Deal and Nolet 1999; Hacker *et al.* 2003), a subducting slab usually has a complicated compositional and thermal structure, i.e. cooler regions are bounded by hotter layers both on the slab surface and inside the slab, like a 'sandwich' (Xiao *et al.* 2006). Previous works demonstrated that significant compositional changes can occur through silicate minerals, melt, metallic glasses, and fluids, not only during compositional gradient driven processes (Richter

*et al.* 2003; Walker *et al.* 1988), i.e. chemical diffusion, but also during temperature gradient driven processes (Lesher and Walker 1986, 1988; Liu *et al.* 2006b; Walker *et al.* 1988), i.e. thermal diffusion. While such a thermal diffusion process occurs within a partially molten material, the process is called thermal migration (Lesher and Walker 1988; Walker *et al.* 1988). When the process occurs in a single mineral phase, or solutions or melts as a result of a temperature gradient, it is termed a Soret effect or Ludig–Soret effect (Lesher and Walker 1986; Walker and DeLong 1982). However, the effects of this kind of disequilibrium in water content and temperature distribution within subducting slabs, on major and trace elements migrations/redistribution, had been ignored so far.

In order to examine the effect from a temperature gradient on intra-slab compositional, especially Nb and Ta, during subduction, we analysed the thermal migration experiment of Huang *et al.* (2009) to gain insight into element redistribution during the subducting process.



### *Experiment design and method*

A detailed description of the experiment can be found in Huang *et al.* (2009). Briefly, a homogeneous andesitic powder (AGV-1; see http://minerals.cr.usgs.gov/ geo_chem_-stand/andesite1.html for complete composition) along with 4 wt-% nanopure $H_2O$ was sealed in a ~20 mm long $Au_{75}Pd_{25}$ capsule with a 3 mm diameter, and welded. The capsule was then placed inside a 5 mm diameter Pt capsule, with a thin graphite liner placed between the two capsules. $CoCl_2.6H_2O$ of 20 mg was placed at the bottom of the Pt capsule to provide water in the outer capsule and act as a $H_2$ getter. The Pt capsule was welded and then put into a crushable MgO column. Finally, the charge along with NaCl–pyrex assemblies with a 10% friction correction were placed into a 3/4″ piston cylinder (Rockland Research). The top of the capsule was located at the centre of the hot spot in the piston cylinder. The experiment ran at 0.5 GPa for 66 days.

According to the temperature profile evaluated from another experiments using double thermocouple arrangements run at the same output power conditions and in the same sample assemblies (Huang *et al.* 2009), the hot end of the sample capsule remained at ~950°C and the cool end at ~350°C, which is also attested through a new 'reaction-progress' thermometer (Watson *et al.* 2002). This experiment was completed in the Department of Geology, University of Illinois at Urbana-Champaign. More details on this experiment, see Huang *et al.* (2009).

### *Analytical method*

The experimental product was cut longitudinally and mounted in epoxy resin, and then polished as a target for composition measurement. Mineral analyses and major element determination were completed using EPMA. Trace elements were analysed by LA-ICP-MS. Detailed conditions were the same as the above analyses on rutile. In order to survey bulk trace elements distributions of experimental product, we collected the composition signals longitudinally every 500 μm from the cool end to the hot end, with laser spot of 60 μm diameter. Meanwhile, we also analysed mineral crystals like plagioclase, amphibole, ilmenite, magnetite, and nearby glasses using a 20 μm diameter laser spot, aiming at the partition coefficients between crystal and melt. $^{43}Ca$ was used as internal standard for bulk and silicate mineral analyses, whereas $^{49}Ti$ was used for Fe–Ti oxides. NIST612 was used as the external calibration standard. Reproducibility of trace element concentrations was assessed to be better than 10%.

### *Thermal migration experimental results*

The experimental product can be divided into three sections based on mineral assemblages (Figure 5A and B): a high-temperature melt section (HMS, 18–10.5 mm), an amphibole present section (APS, 10.5–5.8 mm), and a greenschist section (GS, 5.8–0 mm) from the hot end to the cool end of the capsule.

The HMS consists of mainly quenched melt at the high temperature end of the capsule, with increasing amount of minerals (e.g. apatite, Fe–Ti oxides) as temperature decreases. Both Nb and Ta in the melt have fairly constant Nb and Ta concentrations (Figure 5 and Table 2) that are slightly lower than those of AGV-1 (Nb=15.0 ppm, Ta=0.9 ppm). The Nb/Ta values (16.6–18.7) of the melt are roughly chondritic, and indistinguishable from, or only slightly higher than, that of AGV-1. The Nb and Ta concentrations of Fe–Ti oxides in the HMS decrease with increasing Fe contents in the oxides, consistent with previous experiments (Nielsen and Beard 2000). The highest Nb and Ta concentrations in all Fe–Ti oxides are similar to that of the melt, whereas their Nb/Ta values remain close to that of the

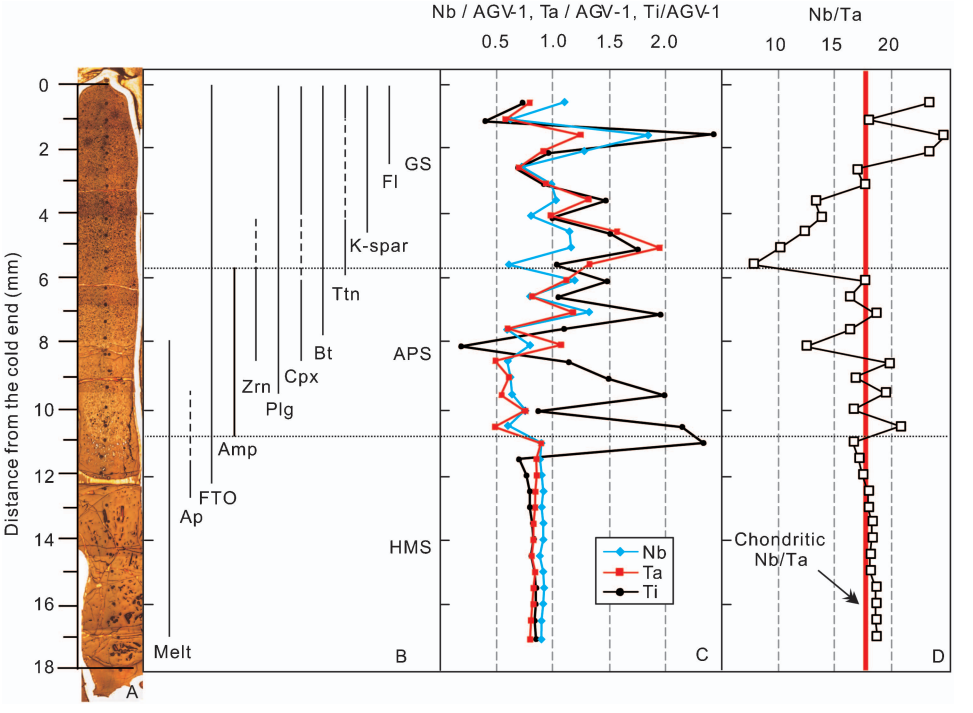


Figure 5. (A) A photomicrograph of the polished surface mount laser pits. (B) A bar graph showing the distribution of minerals in the run product. Dashed lines represent minerals not observed directly due to their rarity. (C) The bulk concentrations of Nb, Ta and Ti normalized to AGV-1. (D) Nb/Ta values on different distance. The lowest Nb/Ta is close to the Ta concentration peak value, whereas the highest Nb/Ta is close to the Nb concentration peak value. Also shown are the chondritic Nb/Ta values (McDonough and Sun 1995) for comparison. Nb, Ta, Ti co-variations and major Nb/Ta fractionation occur at temperatures below 650°C (above ~7 mm) within the titanite stability field. GS, greenschist section; APS, amphibole-present section; HMS, high-temperature melt section; Amp, amphibole; Bt, biotite; Cpx, clinopyroxene; K-spar, potassic feldspar; FTO, Fe–Ti oxides; Plg, plagioclase; Tit, titanite; Zrn, zircon.

Table 2. Concentrations (in ppm) and ratios of run product at different locations.

| Spot | S3 | S4 | S5 | S6 | S7 | S8 | S9 | S10 | S11 |
|---|---|---|---|---|---|---|---|---|---|
| Section | GS | GS | GS | GS | GS | GS | GS | GS | GS |
| Nb | 16.5 | 9.26 | 27.6 | 19.0 | 10.8 | 14.8 | 15.4 | 12.0 | 17.1 |
| Ta | 0.709 | 0.520 | 1.11 | 0.819 | 0.636 | 0.844 | 1.18 | 0.880 | 1.42 |
| Ti | 4507.7 | 2469.1 | 15,257.4 | 6054.8 | 4223.0 | 5770.1 | 9199.7 | 6167.8 | 9511.6 |
| Nb/Ta | 23.3 | 17.8 | 24.8 | 23.2 | 16.9 | 17.5 | 13.1 | 13.6 | 12.1 |
| | S12 | S13 | S14 | S15 | S16 | S17 | S18 | S19 | S20 |
| | GS | GS | APS | APS | APS | APS | APS | APS | APS |
| Nb | 17.4 | 9.02 | 17.7 | 11.8 | 19.6 | 8.72 | 11.8 | 8.67 | 9.24 |
| Ta | 1.75 | 1.20 | 1.00 | 0.730 | 1.06 | 0.537 | 0.960 | 0.438 | 0.552 |
| Ti | 11,025.8 | 6389.8 | 9278.9 | 6489.2 | 12,310.4 | 6286.6 | 1159.6 | 7145.5 | 9237.5 |
| Nb/Ta | 9.96 | 7.54 | 17.6 | 16.2 | 18.5 | 16.2 | 12.3 | 19.8 | 16.7 |
| | S21 | S22 | S23 | S24 | S25 | S26 | S27 | S28 | S29 |
| | APS | APS | APS | HMS | HMS | HMS | HMS | HMS | HMS |
| Nb | 9.37 | 11.2 | 8.94 | 13.3 | 13.3 | 13.3 | 13.6 | 13.5 | 13.50 |
| Ta | 0.484 | 0.677 | 0.432 | 0.802 | 0.776 | 0.767 | 0.761 | 0.757 | 0.743 |
| Ti | 12,454.8 | 5458.3 | 13,465.2 | 14,668.3 | 4384.3 | 4756.6 | 4990.9 | 4968.1 | 5092.0 |
| Nb/Ta | 19.4 | 16.5 | 20.7 | 16.6 | 17.1 | 17.4 | 17.8 | 17.8 | 18.2 |
| | S30 | S31 | S32 | S33 | S34 | S35 | S36 | AGV-1 | |
| | HMS | HMS | HMS | HMS | HMS | HMS | HMS | | |
| Nb | 13.6 | 13.3 | 13.6 | 13.8 | 13.7 | 13.5 | 13.5 | 15.0 | |
| Ta | 0.746 | 0.733 | 0.754 | 0.744 | 0.739 | 0.725 | 0.720 | 0.90 | |
| Ti | 5157.2 | 5026.8 | 5232.9 | 5287.6 | 5330.6 | 5246.7 | 5302.0 | 6293.1 | |
| Nb/Ta | 18.2 | 18.1 | 18.0 | 18.5 | 18.5 | 18.6 | 18.7 | 16.7 | |
| § | S56 | S57 | S54 | S55 | S52 | S53 | S50 | S51 | S48 |
| | Amp | Plg | Amp | Plg | Amp | Plg | Amp | Melt | Amp |
| Nb | 30.1 | 3.78 | 8.58 | 8.42 | 10.8 | 7.33 | 10.6 | 4.78 | 10.7 |
| Ta | 2.01 | 0.387 | 0.505 | 0.628 | 0.613 | 0.513 | 0.498 | 0.255 | 0.552 |
| Nb/Ta | 15.0 | 9.77 | 17.0 | 13.4 | 17.6 | 14.3 | 21.3 | 18.7 | 19.4 |
| $D_{Nb}$ | | | | | | | 2.21 | | 2.49 |
| $D_{Ta}$ | | | | | | | 1.92 | | 2.29 |
| | S49 | S44 | S45 | S42 | S43 | S40 | S41 | S38 | S39 |
| | Melt | Amp | Melt | FTO | Melt | FTO | Melt | FTO | Melt |
| Nb | 4.29 | 13.1 | 11.1 | 0.119 | 11.0 | 11.9 | 11.9 | 9.60 | 12.4 |
| Ta | 0.236 | 0.726 | 0.721 | 0.007 | 0.704 | 0.773 | 0.730 | 0.613 | 0.732 |
| Nb/Ta | 18.2 | 18.0 | 15.4 | 17.0 | 15.6 | 15.4 | 16.3 | 15.7 | 16.9 |
| $D_{Nb}$ | | 1.18 | | 0.011 | | 1.00 | | 0.78 | |
| $D_{Ta}$ | | 1.01 | | 0.014 | | 1.05 | | 0.84 | |

Note: §Analyses using a spot size of 20 μm in diameter. Others are analyses on matrix using a spot size of 60 μm in diameter. Analyses were made at 0.5 mm intervals and are numbered consecutively from cool to hot end of capsule. Abbreviations are shown in the legend of Figure 5.

melt (Table 2), indicating that Fe–Ti oxides cannot dramatically change the Nb/Ta of the bulk sample.

The APS is mainly characterized by the appearance of abundant amphibole along with minor Fe–Ti oxides at the high temperature end of the section. The amount of melt in the matrix decreases, whereas plagioclase, minor clinopyroxene, biotite, and zircon appear consecutively with decreasing temperature (Figure 5B). The Nb concentration of the bulk APS varies significantly from 8.7 to 19.6 ppm. The lowest Nb is observed at ~10.5 mm away from the cool end, close to the boundary with the HMS, followed by increasing but fluctuating Nb as temperature decreases. The Ta

concentration changes similarly but not synchronously with Nb, varying from 0.4 to 1.1 ppm (Figure 5, Table 2). Accordingly, the Nb/Ta value fluctuates significantly (12.3–20.7), indicating decoupling between Nb and Ta.

In the GS, biotite, plagioclase, K-feldspar, and quartz are abundant, with minor clinopyroxene, titanite and fluorite occasionally observed throughout the section. The matrix consists mainly of a fine-grained aggregate of these minerals. The trace element compositions of minerals in this section were not analysed because the grain sizes were too small for LA-ICP-MS analysis ($<10\,\mu m$). No melt was observed in this section being held at a subsolidus temperature. Here the Nb and Ta concentrations as well as Nb/Ta values of the GS fluctuate even more dramatically than those of the APS. The Nb and Ta bulk concentrations range from 5.0 to 27.6 and 0.2 to 1.7 ppm, respectively. The highest Ta concentration is observed close to the APS boundary. As the temperature decreases further, the Ta concentration decreases quickly to values considerably lower than that of the starting materials, indicating net transport of Ta from both the low and high temperature ends of the capsule towards the boundary between the APS and GS fields (Figure 5). By contrast, the Nb concentration increases from its value of 8.7 ppm at the $\sim$10 mm position to 27.6 ppm at the $\sim$2 mm position from the cool end of the capsule (Figure 5). The different migration patterns of Nb and Ta result in a large range in Nb/Ta (7.5–24.8) with suprachondritic Nb/Ta at the lowest temperature and subchondritic Nb/Ta at somewhat higher temperatures (Figure 5 and Table 2).

Huang *et al.* (2009) showed that the distributions of many trace elements (e.g. Rb, Sr, REE, Zr, Hf) reflected diffusion to locations in the experiment where the element had highest bulk partition coefficient. This resulted in relatively smoothly changing element concentrations, following major elements trends which reflected the sequential appearance of minerals with saturation temperature. The trends of Nb, Ta, although somewhat more noisy, appears to also follow migration patterns dictated by minerals with ability to incorporate these elements into their structure (e.g. high partition coefficient).

## Discussion

### *What is responsible for the Nb/Ta fractionation?*

Even though Nb and Ta have long been considered to have identical geochemical behaviours during most mantle processes (Green 1995; Sun and McDonough 1989), considerable Nb/Ta variations have been reported in different rocks formed in various geological settings, including arc rocks (Eggins *et al.* 1997; Munker 1998), oceanic basalt (Niu and Batiza 1997; Sun *et al.* 2003), granitoid suites (Collins *et al.* 1982; Dostal and Chatterjee 2000; Zhao *et al.* 2008), and metamorphic/metasomatic rocks (Aulbach *et al.* 2008; Gao *et al.* 2007; Ionov and Hofmann 1995; Rudnick *et al.* 2000; Xiao *et al.* 2006). Corresponding processes that fractionate Nb and Ta have long been argued. Crystal/melt partitioning and separation has been taken as an important mechanism for Nb and Ta fractionation. Experimental data show that some minerals, such as rutile (Brenan *et al.* 1994; Foley *et al.* 2000; Green and Adam 2003; Green and Pearson 1987; Klemme *et al.* 2005; Schmidt *et al.* 2004; Stalder *et al.* 1998; Xiong *et al.* 2005), titanite (Green and Pearson 1987; Prowatke and Klemme 2003, 2005; Tiepolo *et al.* 2002), ilmenite (Green and Pearson 1987; Klemme *et al.* 2006), and magnetite (Green and Pearson 1987; Nielsen and Beard 2000) favour Ta over Nb, resulting in higher Nb/Ta in melt that separated from or equilibrated with these

mineral crystals, whereas other minerals such as amphibole (Adam *et al.* 1993; Brenan *et al.* 1995; Tiepolo *et al.* 2000), garnet (Green *et al.* 1989, 2000), and clinopyroxene (Green *et al.* 1989, 2000) incorporate more Nb than Ta, leading to lower Nb/Ta in the coexisting melt. Moreover, inasmuch as partial melting of subducting slabs is uncommon in modern subduction conditions while dehydration of subducting slabs is more prevalent, the crucial role of fluids on fractionating Nb and Ta has also been emphasized (Brenan *et al.* 1994; Green 1995; Green and Adam 2003). Present partitioning data indicate that Nb and Ta are fairly high in fluids in the absence of rutile (Stalder *et al.* 1998). Experiments on rutile and aqueous fluid partitioning by Brenan *et al.* (1994) indicated that rutile took up more Nb than Ta, resulting in lower Nb/Ta in the fluids. In contrast, based on a MORB-water metamorphic experiment, Green and Adam (2003) demonstrated $D_{Nb}/D_{Ta}<1$ for rutile, omphacite, garnet, chloritoid, and fluid partitioning, and $D_{Nb}/D_{Ta}>1$ for lawsonite and fluid. In addition, subduction-related or lithospheric mantle metasomatism by carbonatitic melt and/or fluids may also induce fractionation between Nb and Ta (Aulbach *et al.* 2008; Ionov and Hofmann 1995; Ionov *et al.* 1994). Attention has also been paid to the effects of halogen complexes on Nb and Ta (Collins *et al.* 1982; Gao *et al.* 2007; Zhao *et al.* 2008), because the halogen can act as a complexing agent, enhancing Nb and Ta mobility in fluids. Furthermore, the complexes such as $Na_3TaF_8$, $Na_2NbF_7$ can significantly affect on the coherence between Nb and Ta (Green 1995).



### *Dehydration before rutile appears*

Given that rutile is a common minor mineral in most eclogites that dominates the Nb and Ta budgets (Green 1995; Green and Adam 2003; Xiong *et al.* 2005; Zack *et al.* 2002), whereas Nb and Ta are fairly soluble in fluids in the absence of rutile, but are hardly soluble in the presence of rutile ($^{rutile/fluid}D_{Nb,Ta}>100$) (Brenan *et al.* 1994; Stalder *et al.* 1998), major fractionation between Nb and Ta most likely occurred before rutile appeared as previously proposed (Xiao *et al.* 2006). Namely, Nb and Ta fractionate from each other during blueschist to amphibolite transformation at depths below 50 km. Since growing rutile can retain most of the Nb and Ta in fluids (Brenan *et al.* 1994; Stalder *et al.* 1998), the fractionated Nb/Ta was then inherited by rutile as subduction continued. Once Nb and Ta are retained by rutile, the overall fractionated characteristics between Nb and Ta can be well preserved, because rutile solubilities in common mantle or subduction zone fluids at high P and T are rather low (Antignano and Manning 2008; Audétat and Keppler 2005; Tropper and Manning 2005), about one order of magnitude lower than previously estimated based on the weight loss of rutile crystal, ranging from 0.15 to 1.9 wt-% (Ayers and Watson 1993). Therefore, variable Nb and Ta concentrations and Nb/Ta in rutile of CCSD samples at different depths reflect and record the compositional differentiation processes within the subducted slab during early stage dehydration.

Amphibole favours Nb over Ta (Adam *et al.* 1993; Brenan *et al.* 1995; Tiepolo *et al.* 2001), and the ratio between the amphibole-melt partition coefficients of Nb and Ta increase with decreasing Mg number (Foley *et al.* 2002). Consequently, amphibole was taken as the main factor that fractionates Nb from Ta before rutile appears (Xiao *et al.* 2006). This is supported by very high average Nb/Ta (i.e. 48.6) of amphibole in CCSD eclogites (Liang *et al.* 2008), which are dehydration residues and thus should be complementary with fluids in terms of Nb/Ta.

Consistently, rutile in quartz veins precipitated from subduction released fluids has much lower Nb/Ta of about 10 in average (Xiao *et al.* 2006; Zhang *et al.* 2008). These facts imply that significant fractionations of Nb and Ta most likely resulted from the partitioning between amphibole and fluids before rutile appeared.

### *'Thermal' migration*

Examination of Nb-Ta results from the thermal migration experiment show that amphibole plays a major role in controlling the distribution of these elements in the charge. The Nb and Ta concentrations of resultant amphibole ranged from 8.6 to 30.1 and 0.5 to 2.0 ppm, respectively, with Nb/Ta values of 15.0–21.1 in this study (Table 2 and Figure 5). The Nb and Ta concentrations in amphibole were always higher than those in the coexisting matrix, with the partition coefficient of Nb between amphibole and melt, $D_{Nb}$, ranging from 1.18 to 2.49, and the $D_{Ta}$ ranging from 1.01 to 2.29 (Table 2). Amphibole favours Nb over Ta, with $D_{Nb}/D_{Ta}$ ranging from 1.09 to 1.16, although considerably less varied than those that have been measured for the partitioning between amphibole and alkaline basaltic melt (Foley *et al.* 2002; Tiepolo *et al.* 2000). Detailed LA-ICP-MS analyses using a small spot size (20 μm) show that Nb and Ta concentrations of both amphibole and coexisting matrix in the APS region (about 9.0–10.5 mm from the cool end of the capsule) are lower than those of the starting materials (Figure 5). Only one amphibole grain, located near the boundary between the APS and GS, where the matrix is slightly enriched in Nb and Ta, has Nb and Ta concentrations higher than those of AGV-1. These observations imply that major Nb/Ta fractionation was not purely controlled by amphibole.

Our results show that Nb and Ta concentration peaks are associated with Ti peaks between about 7 and 0 mm (corresponding to temperatures of about 650–350°C) (Huang *et al.* 2009), but not at temperatures above 650°C (Figure 5). LA-ICP-MS intensities from spot analyses show that Nb, Ta, and Ti concentration peaks at temperatures below 650°C are due to small mineral grains, suggesting that Nb and Ta were controlled by Ti-rich minerals. Fe–Ti oxides (ilmenite/titanomagnetite) and titanite are the major Ti-bearing minerals at pressures below 1.5 GPa (Liou *et al.* 1998a). Our analyses of Fe–Ti oxides in the HMS show that Fe–Ti oxides have low Nb, Ta concentrations with $D_{Nb}$=0.01–1.0, $D_{Ta}$=0.01–1.1, and $D_{Nb}/D_{Ta}$=0.79–0.95 for Fe–Ti oxides versus granitic melt (Table 2), such that they cannot significantly affect the Nb and Ta budgets and Nb/Ta ratios. In contrast, titanite is known to have very high Nb and Ta concentrations and very low Nb/Ta ratios (<1) (Prowatke and Klemme 2003, 2005; Tiepolo *et al.* 2002). Therefore, a small amount of titanite can dramatically increase bulk Nb and Ta concentrations and decrease Nb/Ta ratios in the system, particularly when amphibole is no longer present. At 0.5 GPa, titanite occurs at temperatures below ~650°C (Liou *et al.* 1998a), which corresponds well to the onset of Nb, Ta, and Ti co-variations in our experiment (Figure 5). Several small grains of titanite were observed using a SEM in the region of the Ta peak.

The highly varied but systematic changes in Ti, Nb, and Ta concentrations indicate that these elements were mobile during the thermal migration experiment. Like other trace elements such as Rb and Sr (Huang *et al.* 2009), concentration distributions are fully consistent with rapid element transportation and incorporation into phases that have the highest partition coefficient. Previous experiments suggested that a partially molten silicate under a temperature gradient should evolve toward fully molten melt at the hot end and fully recrystallized mineral assemblies with no melt at the cool end (Walker *et al.* 1988). Though the thermal migration experiment did not reach this

condition even after 66 days. Nevertheless, the homogeneous Nb, Ta, and Ti in the melt of HMS indicate that the migration of Nb, Ta, and Ti from melt towards the cooler end was limited at least by the end of our experiment. In fact, the Nb, Ta, and Ti concentrations in the melt are close to the starting material, indicating neglectable losses during the whole experiment process. Even if our experiment did not reach perfect dynamic equilibration, such that more Nb, Ta, and Ti might come to concentrate and incorporate into growing mineral phases such as titanite that results in further fractionation if run longer. It has no effect on our conclusion. The current experiment still clearly reveals that with the help of mobile agents, Nb and Ta have different mobilities driven by a large thermal gradient such that Nb and Ta dramatically fractionate from each other (Ding *et al.* 2007). As for the mobile agents, under the experiment condition, supercritical fluids or water-rich melts with properties closer to supercritical $H_2O$ (Huang *et al.* 2009) are among the candidates. Moreover, AGV-1 contains ~425 ppm F, which may have also acted as a complexing agent, to enhance the mobility of Ta and especially Nb (Green 1995).



### *Synchronous mobilities of Nb, Ta and Ti and Nb/Ta fractionation*

Our experiment shows that titanite was an important controlling factor for Nb/Ta fractionation. Given that titanite is also highly enriched in Nb and Ta, it seems that whether rutile appears is not crucial to Nb/Ta fractionation. The most important thing is whether Ti is also mobile and does migrate. Titanium has long been regarded as chemically immobile during subduction (Pearce and Peate 1995). However, a growing number of facts show that Ti can migrate on a distance ranging from a few centimetres to metre scale (Gao *et al.* 2007; van Baalen 1993). In this study, the presence of high-Ti eclogitic layers with a thickness of about 300 m in the CCSD drill hole (Figure 1B) reveals that Ti is indeed mobile, and can move even up to kilometre scale. Ti migration should occur before rutile appeared, as noted above, because of the low solubility of rutile, and restricted fluid flow in low permeability rocks under eclogite conditions (van Baalen 1993). This viewpoint is also supported by other field observation, e.g. Ti contents of mineral, rutile, and titanite abundances and Ti, Nb, and Ta contents in bulk rock decrease from the host rocks towards the segregation (Gao *et al.* 2007).

Our experimental results provide a mechanism that can feasibly account for these observations. The results show that Nb, Ta and Ti co-vary between about 650 and 350°C (corresponding to location of about 7–0 mm, Figure 5) where Nb, Ta and Ti were relatively enriched but dramatic fractionation between Nb, Ta and Ti occurred. By contrast, Nb, Ta, and Ti unsynchronously vary between about 850 and 650°C (corresponding to a location of about 11–7 mm, Figure 5), where Ti was obviously enriched and Nb and Ta were dramatically depleted without major Nb/Ta fractionation. In brief, our experimental results indicate that Nb, Ta, and Ti have synchronous mobilities driven by a thermal gradient towards the cool region (below ~650°C), where Nb/Ta fractionation is easy to arise because of a different thermal migration pattern between Nb and Ta. Also, the Fe–Ti-oxide zone provides a mechanism that can plausibly explain the presence of high-Fe–Ti eclogites that have unusually low Nb, Ta in the CCSD drill hole (Zhang *et al.* 2004).

### *A 'zone defining' dehydration and subsequent partial melting model*

In this paper, systematical studies on Nb and Ta in rutile from CCSD eclogites confirm the observations and model proposed by Xiao *et al.* (2006), which suggested

that major fractionation of Nb and Ta should occur during blueschist to amphibole–eclogite transformation in the absence of rutile during dehydration, and subsequently the fluids with subchondritic Nb/Ta were transported to the wet cooler region and retained by hydrous minerals, ultimately by rutile-bearing eclogites, leaving suprachondritic Nb/Ta in the dry and hotter region. Melting of hydrous rutile-bearing eclogites with initial subchondritic Nb/Ta in the cooler region can produce major components of the CC, i.e. Nb and Ta depletion and subchondritic Nb/Ta. This is supported by our experiment, which provides a mechanism that can feasibly explain why Nb–Ta–Ti-rich components can be transported to the cooler region within the subducting slabs.

Given that there is a large temperature difference between the surface and interior within subducting slabs due to the sustained thermal gradient (Abers *et al.* 2006; Deal and Nolet 1999), dissolved and/or complexing Nb, Ta, and Ti in the released fluids derived from dehydration at the early stage are apt to migrate towards the interior of subducting slabs, where the temperature is below 650°C (Figure 6). This process, driven by thermal gradient, can gradually concentrate Nb, Ta, and Ti in the cooler interior, resulting in their depletions in the hotter surface during subduction. As a consequence, hydrous rutile-rich eclogites with overall subchondritic Nb/Ta are formed in the cooler interior, whereas unhydrous rutile-poor eclogites with highly suprachondritic Nb/Ta that originated from the rocks at the early stage of dehydration are formed in the hotter surface. In the early history of the Earth, dehydration melting is more likely to occur in cool regions as subduction continues, transferring overall subchondritic Nb/Ta characteristics to the CC, although the partition between rutile and melts will slightly increase Nb/Ta in the melts (Foley *et al.* 2000; Klemme *et al.* 2005; Schmidt *et al.* 2004; Xiong *et al.* 2005). Meanwhile, because only little $TiO_2$ is dissolved in the melts during hydrous partial melting of

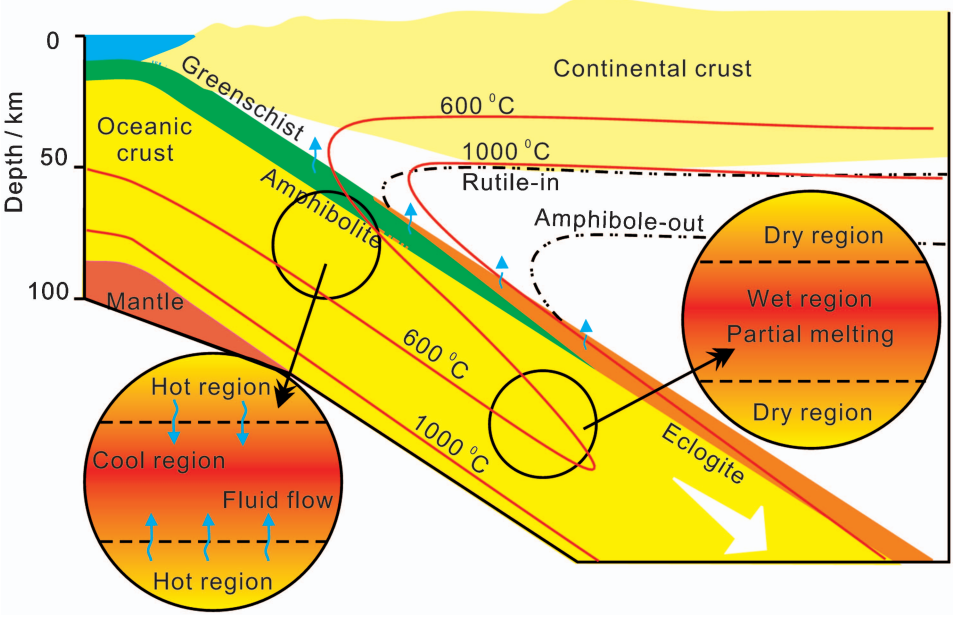


Figure 6. A cartoon showing possible intra-slab dehydration-partial melting processes during subduction, modified from (Abers *et al.* 2006; Hacker *et al.* 2003).

rutile-bearing subducted oceanic crust, and rutile will remain as a residual phase in the eclogites (Gaetani *et al.* 2008), the characteristics of Nb, Ta, and Ti depletion are also transferred to the CC, leaving dry rutile-poor eclogites with highly suprachondritic Nb/Ta and rutile-rich residual eclogites with varied and overall subchondritic Nb/Ta as a complementary reservoir to the CC.

## Conclusions

(1) Systematic Nb and Ta studies on rutile grains from CCSD eclogites show overall inhomoheneous Nb, Ta, and Nb/Ta distributions along the drill hole, and in some cases, also within single grains and between grains at the same depth. The Nb and Ta concentrations range from 6.30 to 1636 and 0.36 to 81.1 ppm, with the average values of 214 and 9.62 ppm, respectively, which is much lower than those from quartz vein, varying from 660 to 2080 and 28.6 to 235 ppm, with the average values of 1564 and 159 ppm, respectively. These, together with the highly varied Nb/Ta, indicate that Nb and Ta are highly mobile at some stage during plate subduction, likely before rutile appears.

(2) Analysis of a thermal migration experiment using wet andesitic powder at 0.5 GPa under a large thermal gradient of 300°C/cm (950–350°C) show dramatic Nb/Ta fractionations. At the high temperature end of the experimental capsule, the melt has a Nb/Ta ratio similar to the starting material. The bulk Nb and Ta concentrations drop suddenly when amphibole appears at 650°C, and then increase undulantly, with fluctuating Nb/Ta. At lower temperature, a Ta concentration peak coupled with low Nb/Ta is observed. Finally, a Nb concentration peak is observed close to the cold end of the capsule. The overall Nb/Ta variation reflects element migration along a temperature gradient, mediated by supercritical fluids or water-rich melts through element partitioning between fluids and minerals.

(3) Both experimental results and field observations indicate that Nb, Ta, and Ti are all mobile, likely driven by a thermal gradient towards the cool region (below ~650°C), where Nb/Ta fractionation is a result of different thermal migration pattern between Nb and Ta.

(4) Both Nb and Ta in rutile from CCSD eclogites and the thermal migration experiment support the 'zone refining' dehydration model (Xiao *et al.* 2006). In detail, at the early stage of subduction, the subducting slabs most likely have a 'sandwich' structure that cooler regions are bounded by hotter layers both on the slab surface and inside the slab. During blueschist to amphibolite transformation, major dehydration occurs in the hotter region, resulting in significant Nb/Ta fractionation due to partitioning between Ti-rich mineral such as amphibole and fluids. This process produces fluids with subchondritic Nb/Ta and leaves a dry and hot region with suprachondritic Nb/Ta. Driven by a thermal gradient, Nb, Ta, and Ti in fluids gradually migrate towards the cooler region. During plate subduction, hydrous rutile-rich eclogites are formed in the cooler region at pressures above 1.5 GPa, inheriting subchondritic Nb/Ta characteristics from the fluids, whereas dry rutile-poor eclogites are formed in the hotter region, with highly suprachondritic Nb/Ta. Finally, dehydration melting is more likely to occur in cool regions as subduction continues in the early history of the

Earth, transferring overall subchondritic Nb/Ta and Nb, Ta, and Ti depletion characteristics to the CC, leaving dry rutile-poor eclogites with highly suprachondritic Nb/Ta and rutile-rich residual eclogites with varied and overall slightly subchondritic Nb/Ta as a complementary reservoir to the CC.

**Acknowledgements**

W.D. Sun was supported by the Nature Science Foundation of China (NSFC) (no. 40525010), Chinese Ministry of Science and Technology (no. 2006CB403505), the Chinese Academy of Sciences and the CAS/SAFEA International Partnership Programme for Creative Research Teams. This project was also sponsored by the China Scholarship Council. This is contribution no. IS-1032 from GIGCAS.



**References**

Abers, G.A., van Keken, P.E., Kneller, E.A., Ferris, A., and Stachnik, J.C., 2006, The thermal structure of subduction zones constrained by seismic imaging: Implications for slab dehydration and wedge flow: Earth and Planetary Science Letters, v. 241, p. 387–397.

Adam, J., Green, T.H., and Sie, S.H., 1993, Proton microprobe determined partitioning of Rb, Sr, Ba, Y, Zr, Nb and Ta between experimentally produced amphiboles and silicate melts with variable F content: Chemical Geology, v. 109, p. 29–49.

Antignano, A., and Manning, C.E., 2008, Rutile solubility in $H_2O$, $H_2O$–$SiO_2$, and $H_2O$–$NaAlSi_3O_8$ fluids at 0.7–2.0GPa and 700–1000 degree C: Implications for mobility of nominally insoluble elements: Chemical Geology, v. 255, p. 283–293.

Audétat, A., and Keppler, H., 2005, Solubility of rutile in subduction zone fluids, as determined by experiments in the hydrothermal diamond anvil cell: Earth and Planetary Science Letters, v. 232, p. 393–402.

Aulbach, S., O'Reilly, S.Y., Griffin, W.L., and Pearson, N.J., 2008, Subcontinental lithospheric mantle origin of high niobium/tantalum ratios in eclogites: Nature Geoscience, v. 1, p. 468–472.

Ayers, J.C., and Watson, E.B., 1993, Rutile solubility and mobility in supercritical aqueous fluids: Contributions to Mineralogy and Petrology, v. 114, p. 321–330.

Barth, M.G., Foley, S.F., and Horn, I., 2002, Partial melting in Archean subduction zones: Constraints from experimentally determined trace element partition coefficients between eclogitic minerals and tonalitic melts under upper mantle conditions: Precambrian Research, v. 113, p. 323–340.

Barth, M.G., McDonough, W.F., and Rudnick, R.L., 2000, Tracking the budget of Nb and Ta in the continental crust: Chemical Geology, v. 165, p. 197–213.

Brenan, J.M., Shaw, H.F., Phinney, D.L., and Ryerson, F.J., 1994, Rutile-aqueous fluid partitioning of Nb, Ta, Hf, Zr, U and Th – implications for high-field strength element depletions in island-arc basalts: Earth and Planetary Science Letters, v. 128, p. 327–339.

Brenan, J.M., Shaw, H.F., Ryerson, F.J., and Phinney, D.L., 1995, Experimental-determination of trace-element partitioning between pargasite and a synthetic hydrous andesitic melt: Earth and Planetary Science Letters, v. 135, p. 1–11.

Carswell, D.A., Wilson, R.N., and Zhai, M., 1996, Ultra-high pressure aluminous titanites in carbonate-bearing eclogites at Shuanghe in Dabieshan, Central China: Mineralogical Magazine, v. 60, p. 461–471.

Collerson, K.D., and Fryer, B.J., 1978, The role of fluids in the formation and subsequent development of early continental crust: Contributions to Mineralogy and Petrology, v. 67, p. 151–167.

Collins, W.J., Beams, S.D., White, A.J.R., and Chappell, B.W., 1982, Nature and origin of A-type granites with particular reference to south eastern Australia: Contributions to Mineralogy and Petrology, v. 80, p. 189–200.

Davidson, J.P., and Turner, S.P., 2006, Controls on magma differentiation at arcs: Crystal redistribution and a role for amphibole: Eos Trans. AGU, v. 87, no. 52, Fall Meet. Suppl., Abstract.

Deal, M.M., and Nolet, G., 1999, Slab temperature and thickness from seismic tomography 2. Izu-Bonin, Japan, and Kuril subduction zones: Journal of Geophysical Research: Solid Earth, v. 104, p. 28803–28812.

Ding, X., Sun, W.D., Huang, F., Lundstrom, C., and Li, J., 2007, Different mobility of Nb and Ta along a thermal gradient: Geochimica et Cosmochimica Acta, v. 71, p. A226.

Dostal, J., and Chatterjee, A.K., 2000, Contrasting behaviour of Nb/Ta and Zr/Hf ratios in a peraluminous granitic pluton (Nova Scotia, Canada): Chemical Geology, v. 163, p. 207–218.

Draut, A.E., Clift, P.D., Hannigan, R.E., Layne, G., and Shimizu, N., 2002, A model for continental crust genesis by arc accretion: rare earth element evidence from the Irish Caledonides: Earth and Planetary Science Letters, v. 203, p. 861–877.

Eggins, S.M., Woodhead, J.D., Kinsley, L.P.J., Mortimer, G.E., Sylvester, P., McCulloch, M.T., Hergt, J.M., and Handler, M.R., 1997, A simple method for the precise determination of ≥40 trace elements in geological samples by ICPMS using enriched isotope internal standardisation: Chemical Geology, v. 134, p. 311–326.

Foden, J.D., and Green, D.H., 1992, Possible role of amphibole in the origin of andesite: Some experimental and natural evidence: Contributions to Mineralogy and Petrology, v. 109, p. 479–493.

Foley, S., Tiepolo, M., and Vannucci, R., 2002, Growth of early continental crust controlled by melting of amphibolite in subduction zones: Nature, v. 417, p. 837–840.

Foley, S.F., Barth, M.G., and Jenner, G.A., 2000, Rutile/melt partition coefficients for trace elements and an assessment of the influence of rutile on the trace element characteristics of subduction zone magmas: Geochimica et Cosmochimica Acta, v. 64, p. 933–938.

Gaetani, G.A., Asimow, P.D., and Stolper, E.M., 2008, A model for rutile saturation in silicate melts with applications to eclogite partial melting in subduction zones and mantle plumes: Earth and Planetary Science Letters, v. 272, p. 720–729.

Gao, J., John, T., Klemd, R., and Xiong, X.M., 2007, Mobilization of Ti–Nb–Ta during subduction: Evidence from rutile-bearing dehydration segregations and veins hosted in eclogites, Tianshan, NW China: Geochimica et Cosmochimica Acta, v. 71, p. 4974–4996.

Green, T.H., 1995, Significance of Nb/Ta as an indicator of geochemical processes in the crust–mantle system: Chemical Geology, v. 120, p. 347–359.

Green, T.H., and Adam, J., 2003, Experimentally-determined trace element characteristics of aqueous fluid from partially dehydrated mafic oceanic crust at 3.0 GPa, 650–700°C: European Journal of Mineralogy, v. 15, p. 815–830.

Green, T.H., Blundy, J.D., Adam, J., and Yaxley, G.M., 2000, SIMS determination of trace element partition coefficients between garnet, clinopyroxene and hydrous basaltic liquids at 2–7.5 GPa and 1080–1200°C: Lithos, v. 53, p. 165–187.

Green, T.H., and Pearson, N.J., 1987, An experimental-study of Nb and Ta partitioning between Ti-rich minerals and silicate liquids at high-pressure and temperature: Geochimica et Cosmochimica Acta, v. 51, p. 55–62.

Green, T.H., Sie, S.H., Ryan, C.G., and Cousens, D.R., 1989, Proton microprobe-determined partitioning of Nb, Ta, Zr, Sr and Y between garnet, clinopyroxene and basaltic magma at high pressure and temperature: Chemical Geology, v. 74, p. 201–216.

Hacker, B.R., Abers, G.A., and Peacock, S.M.., 2003, Subduction factory 1. Theoretical mineralogy, densities, seismic wave speeds, and $H_2O$ contents: Journal of Geophysical Research: Solid Earth, v. 108, DOI: 10.1029/2001JB001127.

Huang, F., Lundstrom, C., Glessner, J., Ianno, A., Boudreau, A., Li, J., Ferre, E., Marshak, S., and DeFrates, J., 2009, Chemical and isotopic fractionation of wet andesite in a temperature gradient: Experiments and models suggesting a new mechanism of magma differentiation: Geochimica et Cosmochimica Acta, v. 73, p. 729–749.

Ionov, D.A., and Hofmann, A.W., 1995, Nb–Ta-rich mantle amphiboles and micas – implications for subduction-related metasomatic trace-element fractionations: Earth and Planetary Science Letters, v. 131, p. 341–356.

Ionov, D.A., Hofmann, A.W., and Shimizu, N., 1994, Metasomatism-induced melting in mantle xenoliths from Mongolia: Journal of Petrology, v. 35, p. 753–785.

Jacob, D.E., Schmickler, B., and Schulze, D.J., 2003, Trace element geochemistry of coesite-bearing eclogites from the Roberts Victor kimberlite, Kaapvaal Craton: Lithos, v. 71, p. 337–351.

Jochum, K.P., Seufert, H.M., Spettel, B., and Palme, H., 1986, The solar system abundances of Nb, Ta and Y and the relative abundances of refractory lithophile elements in differentiated planetary bodies: Geochimica et Cosmochimica Acta, v. 50, p. 1173–1183.

Jochum, K.P., Seuffert, H.M., and Thirlwall, M.F., 1989, High-sensitivity Nb analysis by spark-source mass spectrometry (SSMS) and calibration of XRF Nb and Zr: Chemical Geology, v. 81, p. 1–16.

Kamber, B.S., Ewart, A., Collerson, K.D., Bruce, M.C., and McDonald, G.D., 2002, Fluid-mobile trace element constraints on the role of slab melting and implications for Archaean crustal growth models: Contributions to Mineralogy and Petrology, v. 144, p. 38–56.

Kato, T., Enami, M., and Zhai, M., 1997, Ultra-high-pressure (UHP) marble and eclogite in the Su–Lu UHP terrane, eastern China: Journal of Metamorphic Geology, v. 15, p. 169–182.

Keppler, H., 1996, Constraints from partitioning experiments on the composition of subduction-zone fluids: Nature, v. 380, p. 237–240.

Klemme, S., Gunther, D., Hametner, K., Prowatke, S., and Zack, T., 2006, The partitioning of trace elements between ilmenite, ulvospinel, armalcolite and silicate melts with implications for the early differentiation of the moon: Chemical Geology, v. 234, p. 251–263.

Klemme, S., Prowatke, S., Hametner, K., and Gunther, D., 2005, Partitioning of trace elements between rutile and silicate melts: Implications for subduction zones: Geochimica et Cosmochimica Acta, v. 69, p. 2361–2371.

Lesher, C.E., and Walker, D., 1986, Solution properties of silicate liquids from thermal diffusion experiments: Geochimica et Cosmochimica Acta, v. 50, p. 1397–1411.

———, 1988, Cumulate maturation and melt migration in a temperature-gradient: Journal of Geophysical Research, v. 93, p. 10295–10311.

Li, S., Jagoutz, E., Chen, Y., and Li, Q., 2000, Sm–Nd and Rb–Sr isotopic chronology and cooling history of ultrahigh pressure metamorphic rocks and their country rocks at Shuanghe in the Dabie Mountains, central China: Geochimica et Cosmochimica Acta, v. 64, p. 1077–1093.

Li, S., Wang, S., Chen, Y., Liu, D., Ji, Q., Zhou, H., and Zhang, Z., 1994, Excess argon in phengite from eclogite; evidence from dating of eclogite minerals by Sm–Nd, Rb–Sr and (super 40) Ar/(super 39) Ar methods: Chemical Geology, v. 112, p. 343–350.

Li, S., Xiao, Y., Liou, D., Chen, Y., Ge, N., Zhang, Z., Sun, S.-S., Cong, B., Zhang, R., Hart, S.R., and Wang, S., 1993, Collision of the North China and Yangtse blocks and formation of coesite-bearing eclogites; timing and processes: Chemical Geology, v. 109, p. 89–111.

Liang, J.L., Sun, W.D., and Sun, X.M., 2008, Amphibole controlled Nb/Ta fractionation during subduction: Geochimica et Cosmochimica Acta, v. 72, p. A550.

Liou, J.G., Zhang, R.Y., Ernst, W.G., Liu, J., and McLimans, R., 1998a, Mineral parageneses in the Piampaludo eclogitic body, Gruppo di Voltri, Western Ligurian Alps: Schweizerische Mineralogische und Petrographische Mitteilungen, v. 78, p. 317–335.

Liou, J.G., Zhang, R.Y., Ernst, W.G., Rumble, D., and Maruyama, S., 1998b, High-pressure minerals from deeply subducted metamorphic rocks: Ultrahigh-Pressure Mineralogy, v. 37, p. 33–96.

Liu, D., Jian, P., Kroner, A., and Xu, S., 2006a, Dating of prograde metamorphic events deciphered from episodic zircon growth in rocks of the Dabie–Sulu UHP complex, China: Earth and Planetary Science Letters, v. 250, p. 650–666.

Liu, Y., Liu, C.T., George, E.P., and Wang, X.Z., 2006b, Thermal diffusion and compositional inhomogeneity in cast $Zr_{50}Cu_{50}$ bulk metallic glass: Applied Physics Letters, v. 89, p. 051919–3.

Martin, H., 1999, Adakitic magmas: Modern analogues of Archaean granitoids: Lithos, v. 46, p. 411–429.

McDonough, W.F., 1991, Partial melting of subducted oceanic-crust and isolation of its residual eclogitic lithology: Philosophical Transactions of the Royal Society of London Series A: Mathematical Physical and Engineering Sciences, v. 335, p. 407–418.

McDonough, W.F., and Sun, S.S., 1995, The composition of the Earth: Chemical Geology, v. 120, p. 223–253.

Munker, C., 1998, Nb/Ta fractionation in a Cambrian arc back arc system, New Zealand: Source constraints and application of refined ICPMS techniques: Chemical Geology, v. 144, p. 23–45.

Munker, C., Pfander, J.A., Weyer, S., Buchl, A., Kleine, T., and Mezger, K., 2003, Evolution of planetary cores and the earth-moon system from Nb/Ta systematics: Science, v. 301, p. 84–87.

Nielsen, R.L., and Beard, J.S., 2000, Magnetite–melt HFSE partitioning: Chemical Geology, v. 164, p. 21–34.

Niu, Y.L., and Batiza, R., 1997, Trace element evidence from seamounts for recycled oceanic crust in the eastern Pacific mantle: Earth and Planetary Science Letters, v. 148, p. 471–483.

Pearce, J.A., and Peate, D.W., 1995, Tectonic implications of the composition of volcanic arc magmas: Annual Review of Earth and Planetary Sciences, v. 23, p. 251–285.

Plank, T., and Langmuir, C.H., 1998, The chemical composition of subducting sediment and its consequences for the crust and mantle: Chemical Geology, v. 145, p. 325–394.

Prowatke, S., and Klemme, S., 2003, Melt compositional controls on trace element partitioning: An experimental study of titanite/melt partitioning: Geochimica et Cosmochimica Acta, v. 67, p. A385–A385.

———, 2005, Effect of melt composition on the partitioning of trace elements between titanite and silicate melt: Geochimica et Cosmochimica Acta, v. 69, p. 695–709.

Rapp, R.P., Shimizu, N., and Norman, M.D., 2003, Growth of early continental crust by partial melting of eclogite: Nature, v. 425, p. 605–609.

Rapp, R.P., and Watson, E.B., 1995, Dehydration Melting of Metabasalt at 8–32 kBar: Implications for continental growth and crust–mantle recycling: J. Petrology, v. 36, p. 891–931.

Rapp, R.P., Watson, E.B., and Miller, C.F., 1991, Partial melting of amphibolite eclogite and the origin of Archean trondhjemites and tonalites: Precambrian Research, v. 51, p. 1–25.

Richter, F.M., Davis, A.M., DePaolo, D.J., and Watson, E.B., 2003, Isotope fractionation by chemical diffusion between molten basalt and rhyolite: Geochimica et Cosmochimica Acta, v. 67, p. 3905–3923.

Rudnick, R.L., Barth, M., Horn, I., and McDonough, W.F., 2000, Rutile-bearing refractory eclogites: Missing link between continents and depleted mantle: Science, v. 287, p. 278–281.

Rudnick, R.L., Gao, S., Heinrich, D.H., and Turekian, K.K., 2003, Composition of the continental crust, treatise on geochemistry: Oxford, Pergamon.

Schmidt, M.W., Dardon, A., Chazot, G., and Vannucci, R., 2004, The dependence of Nb and Ta rutile-melt partitioning on melt composition and Nb/Ta fractionation during subduction processes: Earth and Planetary Science Letters, v. 226, p. 415–432.

Shannon, R.D., 1976, Revised effective ionic-radii and systematic studies of interatomic distances in halides and chalcogenides: Acta Crystallographica Section, v. 32, p. 751–767.

Spandler, C., Hermann, J., Arculus, R., and Mavrogenes, J., 2003, Redistribution of trace elements during prograde metamorphism from lawsonite blueschist to eclogite facies; implications for deep subduction-zone processes: Contributions to Mineralogy and Petrology, v. 146, p. 205–222.

Stalder, R., Foley, S.F., Brey, G.P., and Horn, I., 1998, Mineral aqueous fluid partitioning of trace elements at 900–1200°C and 3.0–5.7 GPa: New experimental data for garnet, clinopyroxene, and rutile, and implications for mantle metasomatism: Geochimica et Cosmochimica Acta, v. 62, p. 1781–1801.

Su, S.G., Liou, J.G., You, Z.D., Liang, F.H., and Zhang, Z.M., 2005, Petrologic study of ultrahigh-pressure metamorphic cores from 100 to 2000 m depth in the main hole of the Chinese Continental Scientific Drilling Project, Eastern China: International Geology Review, v. 47, p. 1144–1159.

Sun, S.S., and McDonough, W.F., 1989, Chemical and isotopic systematics of oceanic basalts; implications for mantle composition and processes, *in* Saunders, A.D., and Norry, M.J., eds., Magmatism in the ocean basins: London, Geological Society of London, v. 42, p. 313–345.

Sun, W., Bennett, V.C., Eggins, S.M., Arculus, R.J., and Perfit, M.R., 2003, Rhenium systematics in submarine MORB and back-arc basin glasses: Laser ablation ICP-MS results: Chemical Geology, v. 196, p. 259–281.

Sun, W.D., Williams, I.S., and Li, S.G., 2002, Carboniferous and Triassic eclogites in the western Dabie Mountains, East-Central China: Evidence for protracted convergence of the North and South China Blocks: Journal of Metamorphic Geology, v. 20, p. 873–886.

Sun, X.M., Tang, Q., Sun, W.D., Xu, L., Zhai, W., Liang, J.L., Liang, Y.H., Shen, K., Zhang, Z.M., Zhou, B., and Wang, F.Y., 2007, Monazite, iron oxide and barite exsolutions in apatite aggregates from CCSD drillhole eclogites and their geological implications: Geochimica et Cosmochimica Acta, v. 71, p. 2896–2905.

Tatsumi, Y., Takahashi, N., Kodaira, S., and Kaneda, Y., 2006, Arc evolution and continental crust formation at the Izu–Bonin–Mariana arc system: Geochimica et Cosmochimica Acta, v. 70, p. A638.

Tiepolo, M., Bottazzi, P., Foley, S.F., Oberti, R., Vannucci, R., and Zanetti, A., 2001, Fractionation of Nb and Ta from Zr and Hf at mantle depths: the role of titanian pargasite and kaersutite: Journal of Petrology, v. 42, p. 221–232.

Tiepolo, M., Oberti, R., and Vannucci, R., 2002, Trace-element incorporation in titanite: Constraints from experimentally determined solid/liquid partition coefficients: Chemical Geology, v. 191, p. 105–119.

Tiepolo, M., Vannucci, R., Oberti, R., Foley, S., Bottazzi, P., and Zanetti, A., 2000, Nb and Ta incorporation and fractionation in titanian pargasite and kaersutite: Crystal–chemical constraints and implications for natural systems: Earth and Planetary Science Letters, v. 176, p. 185–201.

Tong, L.X., Jahn, B.M., Iizuka, Y., and Xu, Z.Q., 2007, Assemblages and textural evolution of UHP eclogites from the Chinese Continental Scientific Drilling main hole: International Geology Review, v. 49, p. 73–89.

Tropper, P., and Manning, C.E., 2005, Very low solubility of rutile in $H_2O$ at high pressure and temperature, and its implications for Ti mobility in subduction zones: American Mineralogist, v. 90, p. 502–505.

Tsujimori, T., 2002, Prograde and retrograde P–T paths of the late Paleozoic glaucophane eclogite from the Renge metamorphic belt, Hida Mountains, southwestern Japan: International Geology Review, v. 44, p. 797–818.

van Baalen, M.R., 1993, Titanium mobility in metamorphic systems: A review: Chemical Geology, v. 110, p. 233–249.

Walker, D., and DeLong, S.E., 1982, Soret separation of mid-ocean ridge basalt magma: Contributions to Mineralogy and Petrology, v. 79, p. 231–240.

Walker, D., Jurewicz, S., and Watson, E.B., 1988, Adcumulus dunite growth in a laboratory thermal gradient: Contributions to Mineralogy and Petrology, v. 99, p. 306–319.

Wang, Q.X., Shi, Q.C., Lin, W., and Guo, J.H., 2008, Exhumation of the Dabie UHP terrane, China: International Geology Review, v. 50, p. 15–31.

Wang, R.C., Wang, S., Qiu, J.S., and Ni, P., 2005, Rutile in the UHP eclogites from the CCSD main drillhole (Donghai, eastern China): Trace-element geochemistry and metallogenetic implications: Acta Petrologica Sinica, v. 21, p. 465–474.

Wang, X., Liou, J.G., and Mao, H.K., 1989, Coesite-bearing eclogite from the Dabie Mountains in central China: Geology, v. 17, p. 1085–1088.

Watson, E.B., Wark, D.A., Price, J.D., and van Orman, J.A., 2002, Mapping the thermal structure of solid-media pressure assemblies: Contributions to Mineralogy and Petrology, v. 142, p. 640–652.

Xiao, Y., Sun, W., Hoefs, J., Simon, K., Zhang, Z., Li, S., and Hofmann, A.W., 2006, Making continental crust through slab melting: Constraints from niobium-tantalum fractionation in UHP metamorphic rutile: Geochimica et Cosmochimica Acta, v. 70, p. 4770–4782.

Xiong, X.-.L., 2006, Trace element evidence for growth of early continental crust by melting of rutile-bearing hydrous eclogite: Geology, v. 34, p. 945–948.

Xiong, X.L., Adam, J., and Green, T.H., 2005, Rutile stability and rutile/melt HFSE partitioning during partial melting of hydrous basalt: Implications for TTG genesis: Chemical Geology, v. 218, p. 339–359.

Xu, Z.Q., 2004, The scientific goals and investigation progresses of the Chinese Continental Scientific Drilling Project: Acta Petrologica Sinica, v. 20, p. 1–8.

Xu, Z.Q., Yang, W.C., Zhang, Z.M., and Yang, T.N., 1998, Scientific significance and site-selection researches of the first Chinese Continental Scientific Deep Drillhole: Continental Dynamics, v. 3, p. 1–13.

Ye, K., Cong, B.L., and Ye, D.I., 2000, The possible subduction of continental material to depths greater than 200 km: Nature, v. 407, p. 734–736.

You, Z.D., Su, S.G., Liang, F.H., and Zhang, Z.M., 2004, Petrography and metamorphic deformational history of the ultrahigh-pressure metamorphic rocks from the 100 similar to 2000 m core of Chinese Continental Scientific Drilling, China: Acta Petrologica Sinica, v. 20, p. 43–52.

———, 2005, The metamorphic evolution of the eclogitic rocks in the main hole of the Chinese Continental Scientific Drilling Project: An elucidation on the uplift processes of the ultrahigh-pressure metamorphic terrane: Acta Petrologica Sinica, v. 21, p. 381–388.

Zack, T., Kronz, A., Foley, S.F., and Rivers, T., 2002, Trace element abundances in rutiles from eclogites and associated garnet mica schists: Chemical Geology, v. 184, p. 97–122.

Zhang, R.Y., Hirajima, T., Banno, S., Cong, B., and Liou, J.G., 1995, Petrology of ultrahigh-pressure rocks from the southern Su–Lu region, eastern China: Journal of Metamorphic Geology, v. 13, p. 659–675.

Zhang, R.Y., and Liou, J.G., 1996, Coesite inclusions in dolomite from eclogite in the southern Dabie Mountains, China: The significance of carbonate minerals in UHPM rocks: American Mineralogist, v. 81, p. 181–186.

Zhang, R.Y., Yang, J.S., Wooden, J.L., Liou, J.G., and Li, T.F., 2005a, U–PbSHRIMP geochronology of zircon in garnet peridotite from the Sulu UHP terrane, China: Implications for mantle metasomatism and subduction-zone UHP metamorphism: Earth and Planetary Science Letters, v. 237, p. 729–743.

Zhang, Z.-M., Shen, K., Sun, W.-D., Liu, Y.-S., Liou, J.G., Shi, C., and Wang, J.-L., 2008, Fluids in deeply subducted continental crust: Petrology, mineral chemistry and fluid inclusion of UHP metamorphic veins from the Sulu Orogen, Eastern China: Geochimica et Cosmochimica Acta, v. 72, p. 3200–3228.

Zhang, Z.M., Xiao, Y.L., Liu, F.L., Liou, J.G., and Hoefs, J., 2005b, Petrogenesis of UHP metamorphic rocks from Qinglongshan, southern Sulu, East-Central China: Lithos, v. 81, p. 189–207.

Zhang, Z.M., Xu, Z.Q., Liu, F.L., You, Z.D., Shen, K., Yang, J.S., Li, T.F., and Chen, C.Z., 2004, Geochemistry of eclogites from the main hole (100 similar to 2050 m) of the Chinese Continental Scientific Drilling Project: Acta Petrologica Sinica, v. 20, p. 27–42.

Zhang, Z.M., Xu, Z.Q., and Xu, H.F., 2000, Petrology of ultrahigh-pressure eclogites from the ZK703 drillhole in the Donghai, Eastern China: Lithos, v. 52, p. 35–50.

Zhang, Z.M., Zhang, J.F., You, Z.D., and Shen, K., 2005c, Ultrahigh-pressure metamorphic P–T–t path of the Sulu orogenic belt, Eastern Central China: Acta Petrologica Sinica, v. 21, p. 257–270.

Zhao, Z.H., Xiong, X.L., Wang, Q., and Qiao, Y.L., 2008, Some aspects on geochemistry of Nb and Ta: Geochimica, v. 37, p. 304–320.

Zheng, Y.F., Fu, B., Gong, B., and Li, L., 2003, Stable isotope geochemistry of ultrahigh pressure metamorphic rocks from the Dabie–Sulu Orogen in China: implications for geodynamics and fluid regime: Earth-Science Reviews, v. 62, p. 105–161.